Supplementary Information (SI) for Energy & Environmental Science.

Supporting Information

Spatial Structure Regulation Strategy Modulated Solubility and Compactness of Novel Face-on Oriented Bisphosphonate-Anchored SAMs for Efficient Inverted Perovskite Solar Cells

Weixu Duan,[1a] Kai Chen,[1*a] Bingxue Pi,[a] Shaojian Li,[a] Zedong Lin,[c] Yuehua Pan,[a] Haiqian Ling,[a] Desheng Li,[a] Cong Liu,[*a] Liwei Zhou,[a] Tao Liu,[*a] Fan Wu,[a] Xiangwen Guo,[a] Bingsuo Zou,[a] and Xiaotian Hu[*b]

---

a., Guangxi Key Laboratory of Processing for Non-ferrous Metals and Featured Materials, School of Resources, Environment and Materials, Guangxi University, Nanning 530004, China. E-mail: chenkai@gxu.edu.cn, liutaozhx@gxu.edu.cn, congliu@gxu.edu.cn

b., Institute of Polymers and Energy Chemistry (IPEC)/Film Energy Chemistry for Jiangxi Provincial Key Laboratory (FEC), Nanchang University, 999 Xuefu Avenue, Nanchang, 330031, China. E-mail: happyhu@ncu.edu.cn

c., School of Materials Science and Engineering, Taizhou University, Taizhou 318000, China.

Materials and Synthesis.

Isopropanol (IPA, ≥99.5%), N, N-dimethylformamide (DMF, 99.8%), dimethyl sulfoxide (DMSO, ≥99.9%), chlorobenzene (CB, 99.8%) and alumina nanoparticles (Al_2O_3 20 wt.% in IPA, <50 nm particle size) were purchased from Sigma Aldrich. Ethyl alcohol (≥99.8%) was purchased from Aladdin. Lead (II) iodide (PbI_2, 99.999%) was purchased from Advanced Election Technology Co. Ltd. Methylammonium bromide (MABr, 99.5%), methylammonium chloride (MACl, 99.5%), cesium iodide (CsI, 99.999%), phenylethyl ammonium bromide (PEABr, 99.5%), phenyl-C61-butyric acid methyl-ester ($PC_{61}BM$, 99%), fullerene (C_{60}, 99%) and bathocuproine (BCP, 99%) were purchased from Xi'an Yuri Solar Co. Ltd. [4-(3,6-dimethyl-9H-carbazol9yl)butyl]phosphonic acid (Me-4PACz, >99.0%) was purchased from Tokyo Chemical Industry. Formamidinium iodide (FAI) was purchased from Greatcell Solar Materials. All materials were used as received.

The synthetic routes to CDC, TDC, and TDT were illustrated in **Scheme S1.** The preparation details were described as follows.

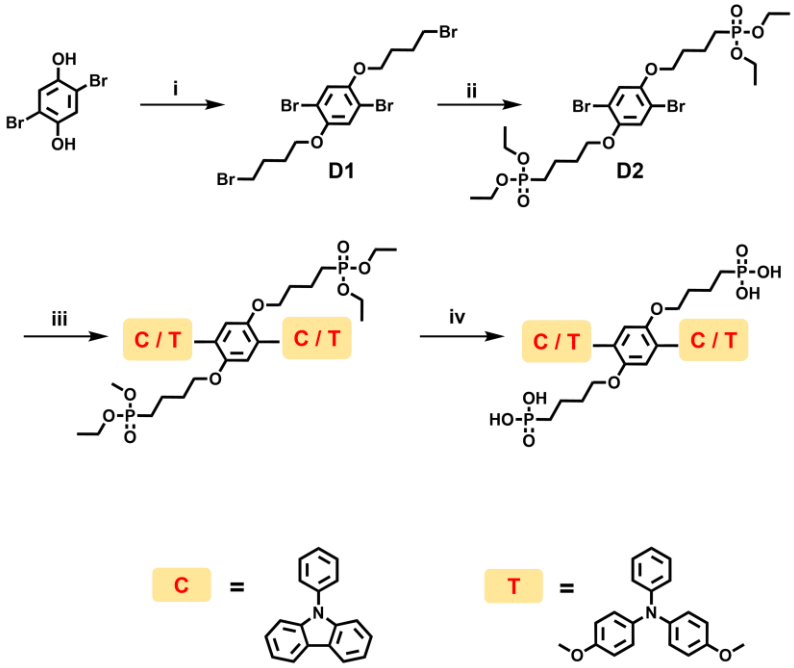

Scheme S1. Synthetic route to CDC, TDC and TDT. Reagents and conditions:

(i) $C_4H_8Br_2$, K_2CO_3, acetone, 90 °C, reflux, 24 h; (ii) $P(OEt)_3$, 145 °C, reflux, 16 h;

(iii) $Pd(PPh_3)_4$, Aliquat 336, 2M K_2CO_3, toluene, 90 °C , dark, 12 h;

(iv) $(CH_3)_3SiBr$, CH_2Cl_2, 25 °C, 18 h.

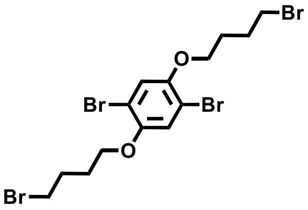

Synthesis of 1,4-dibromo-2,5-bis(4-bromobutoxy) benzene (D1).

2,5-dibromobenzene-1,4-diol (2.68 g, 10.00 mmol), 1,4-dibromobutane (4.15 mL, 27.00 mmol), and potassium carbonate (6.91 g, 50.00 mmol) were dissolved in anhydrous acetone (50.00 mL). The resulting solution was refluxed overnight at 90 °C under argon atmosphere. The resulting mixture was concentrated under vacuum and then redissolved in dichloromethane and washed with water. After water was dried over $NaSO_4$ and dichloromethane was removed under vacuum, the crude product was purified with silica-gel column chromatography (petroleum: dichloromethane = 3:1, v/v) to give **D1** as a white powder. Yield: 4.33 g (80.5%). ^{1}H NMR (600 MHz, $CDCl_3$) δ = 7.17 (s, 2H), 3.98 (t, 4H), 3.53 (t, 4H), 2.16 – 2.10 (m, 4H), 2.00 – 1.95 (m, 4H).

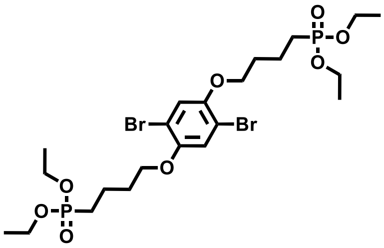

Synthesis of tetraethyl (((2,5-dibromo-1,4-phenylene)bis(oxy))bis(butane-4,1-diyl))bis(phosphonate) (D2).

D1 (1.50 g, 2.79 mmol), triethyl phosphite (3.80 mL, 22.3 mmol) were added into a 50.00mL round-bottom flask. The resulting solution was refluxed for 16 h at 145 °C The resulting mixture was redissolved in dichloromethane and washed with water. After water was dried over Na_2SO_4 and dichloromethane was removed under vacuum, the crude product was purified with silica-gel column chromatography (ethyl acetate) to give a white solid. Yield: 1.33 g (73.2%). ^{1}H NMR (600 MHz, $CDCl_3$) δ = 7.10 (s, 2H), 4.26 – 4.06 (m, 8H), 3.99 (t, 4H), 2.01 – 1.73 (m, 12H), 1.35 (t, 12H).

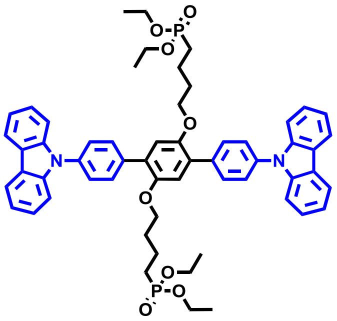

CDC-P

Synthesis of CDC-P.

D2 (1.96 g, 3.0 mmol), 9-(4-(4,4,5,5-tetramethyl-1,3,2-dioxaborolan-2-yl)phenyl)-9H-carbazole(2.58 g, 7.0 mmol) , Pd(PPh$_3$)$_4$ (0.16 g, 0.14mmol) , Aliquat 336 (7.0 mg) in a two phase solvent of 2M K$_2$CO$_3$ (3.0 mL) and toluene (9.0 mL) was heated to 90 °C and stirred in dark for 12 h. After cooling, the mixture was washed with brine and dried with anhydrous Na$_2$SO$_4$. The residue was purified by silica-gel column chromatography to give a white solid. Yield: 2.28 g (77.8%). ^{1}H NMR (600 MHz, CDCl$_3$) δ = 8.18 (d, 4H), 7.88 (d, 4H), 7.68 (d, 4H), 7.56 (d, 4H), 7.46 (t, 4H), 7.33 (t, 4H), 7.16 (s, 2H), 4.15 – 3.99 (m, 12H), 1.85 (t, 12H), 1.24 (t, 12H). ^{13}C NMR (151 MHz, CDCl$_3$) δ = 150.30, 140.84, 137.23, 136.63, 130.93, 130.19, 126.49, 125.99, 123.47, 120.35, 120.02, 116.08, 109.93, 77.30, 77.09, 76.88, 68.84, 61.52, 30.14, 25.87, 24.93, 19.46, 16.46.

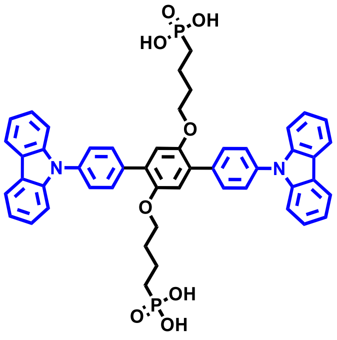

CDC

Synthesis of CDC.

CDC-P (1.17 g, 1.2 mmol) was dissolved in anhydrous dichloromethane (20 mL) under nitrogen atmosphere and trimethylbromosilane (4.0 mL) was added dropwise. Reaction was stirred for 18 h at room temperature. Afterwards solvent was partially distilled off under reduced pressure, and the liquid residue was dissolved in methanol (10 ml).

Finally, distilled water was dropped slowly until a large amount of solid was produced. The solid was filtered off and washed with water to give a white solid of CDC. Yield: 0.92 g (88.63%). ^{1}H NMR (600 MHz, DMSO) δ = 8.26 (d, 4H), 7.95 (d, 4H), 7.70 (d, 4H), 7.57 – 7.43 (m, 8H), 7.30 (dd, 6H), 4.11 (t, 4H), 1.85 – 1.78 (m, 4H), 1.69 (d, 4H), 1.64 – 1.55 (m, 4H). ^{13}C NMR (151 MHz, DMSO) δ = 140.51, 131.48, 126.82, 126.50, 123.26, 121.01, 120.57, 110.29, 30.09, 20.07. ^{31}P NMR (243 MHz, DMSO) δ = 26.55. HRMS (ESI-TOF) m/z: [M+H]$^{+}$ Calculated for $C_{50}H_{46}N_2O_8P_2$: 865.86: Found: 865.28.

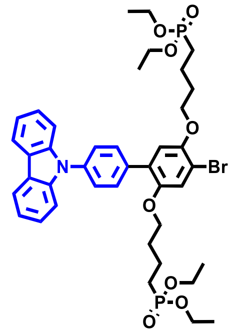

CD-P

Synthesis of CD-P

D2 (1.96 g, 3.0 mmol), 9-(4-(4,4,5,5-tetramethyl-1,3,2-dioxaborolan-2-yl)phenyl)-9H-carbazole(1.29 g, 3.5 mmol), $Pd(PPh_3)_4$ (0.08 g, 0.07 mmol), Aliquat 336 (3.5 mg) in a two phase solvent of 2M K_2CO_3 (2.0 mL) and toluene (4.5 mL) was heated to 90 °C and stirred in dark for 12 h. After cooling, the mixture was washed with brine and dried with anhydrous Na_2SO_4. The residue was purified by column chromatography to give a white solid. Yield: 1.96 g (80.16%). ^{1}H NMR (600 MHz, $CDCl_3$) δ = 8.15 (d, 2H), 7.74 (d, 2H), 7.61 (d, 2H), 7.50 (d, 2H), 7.43 (t, 2H), 7.30 (t, 2H), 7.21 (s, 1H), 7.00 (s, 1H), 4.04 (ddt, 12H), 1.94 – 1.83 (m, 8H), 1.75 (d, 4H), 1.33 (t, 6H), 1.22 (t, 6H). ^{13}C NMR (151 MHz, $CDCl_3$) δ = 150.26, 149.86, 140.67, 136.65, 130.78, 129.85, 129.72, 126.36, 125.96, 123.39, 120.27, 120.02, 118.19, 116.25, 111.73, 109.82, 69.43, 68.70, 61.61, 61.24, 29.88, 25.75, 24.82, 19.39, 16.63, 16.37.

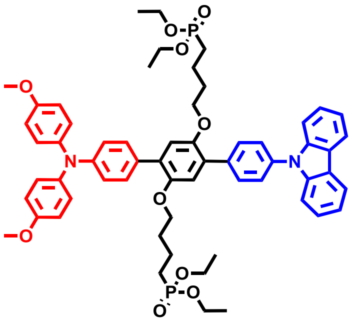

TDC-P

Synthesis of TDC-P.

CD-P (1.2 g, 1.5 mmol), 4-methoxy-N-(4-methoxyphenyl)-N-(4-(4,4,5,5-tetramethyl-1,3,2-dioxaborolan-2-yl)phenyl)aniline (0.86 g, 2.0 mmol) , $Pd(PPh_3)_4$ (0.08 g, 0.07 mmol) , Aliquat 336 (2.0 mg) in a two phase solvent of 2M K_2CO_3 (1.0 mL) and toluene (3.0 mL) was heated to 90 °C and stirred in dark for 12 h. After cooling, the mixture was washed with brine and dried with anhydrous Na_2SO_4. The residue was purified by column chromatography to give a white solid. Yield: 1.33 g (85.4%). ^{1}H NMR (600 MHz, $CDCl_3$) δ = 8.16 (d, 2H), 7.83 (d, 2H), 7.63 (d, 2H), 7.53 (d, 2H), 7.43 (d, 2H), 7.30 (t, 1H), 7.17 – 6.84 (m, 12H), 4.09 – 3.99 (m, 6H), 3.82 (s, 3H), 1.89 – 1.75 (m, 6H), 1.30 – 1.21 (m, 6H). ^{13}C NMR (151 MHz, $CDCl_3$) δ = 155.94, 150.23, 140.84, 137.43, 136.37, 130.96, 129.46, 126.76, 126.41, 125.96, 123.42, 120.30, 119.84, 116.11, 115.77, 114.74, 109.93, 77.31, 77.10, 76.89, 68.74, 61.49, 60.41, 55.51, 30.12, 29.72, 25.84, 24.91, 21.06, 19.44, 16.49, 14.22.

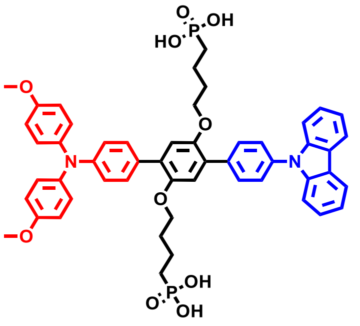

TDC

Synthesis of TDC.

TDC-P (1.24 g, 1.2 mmol) was dissolved in anhydrous dichloromethane (20 mL) under nitrogen atmosphere and trimethylbromosilane (4 mL) was added dropwise. Reaction was stirred for 18 h at room temperature. Afterwards solvent was partially distilled off under reduced pressure, and the liquid residue was dissolved in methanol (10 ml).

Finally, distilled water was dropped slowly until a large amount of solid was produced. The solid was filtered off and washed with water to give a white solid of TDC. Yield: 1.05 g (94.5%). ^{1}H NMR (600 MHz, DMSO) δ = 8.29 (d, 2H), 7.92 (d, 2H), 7.70 (d, 2H), 7.55 – 7.47 (m, 6H), 7.33 (t, 2H), 7.18 (s, 1H), 7.10 (d, 5H), 6.96 (d, 4H), 6.85 (d, 1H), 4.12 – 3.99 (m, 4H), 3.78 (s, 6H), 1.79 (s, 4H), 1.61 (ddd, 8H). ^{13}C NMR (151 MHz, DMSO) δ = 156.30, 150.15, 147.94, 140.58, 130.43, 127.17, 126.47, 121.04, 119.16, 115.43, 110.30, 68.54, 55.78, 55.72, 30.14, 11.87, 10.96. ^{31}P NMR (243 MHz, DMSO) δ = 26.30. HRMS (ESI-TOF) m/z: $[M+Na]^+$ Calculated for $C_{52}H_{52}N_2O_{10}P_2$: 949.91: Found: 949.30.

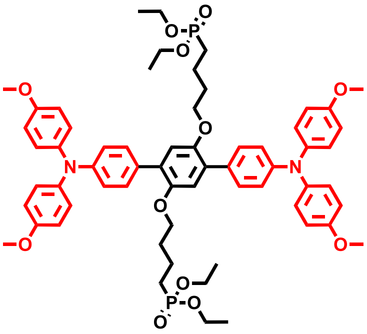

TDT-P

Synthesis of TDT-P.

D2 (1.96 g, 3.0 mmol), 4-methoxy-N-(4-methoxyphenyl)-N-(4-(4,4,5,5-tetramethyl-1,3,2-dioxaborolan-2-yl)phenyl)aniline (3.02 g, 7.0 mmol), $Pd(PPh_3)_4$ (0.16 g, 0.07 mmol) , Aliquat 336 (7.0 mg) in a two phase solvent of 2M K_2CO_3 (3.0 mL) and toluene (9.0 mL) was heated to 90 °C and stirred in dark for 12 h. After cooling, the mixture was washed with brine and dried with anhydrous Na_2SO_4. The residue was purified by column chromatography to give a white solid. Yield: 2.88 g (87.3%). ^{1}H NMR (600 MHz, $CDCl_3$) δ = 7.41 (s, 4H), 6.93 (dd, 20H), 4.16 – 3.69 (m, 24H), 1.84 – 1.68 (m, 12H), 1.30 – 1.21 (m, 12H). ^{13}C NMR (151 MHz, $CDCl_3$) δ = 150.16, 129.87, 126.65, 119.78, 115.84, 114.66, 68.65, 61.46, 55.50, 30.10, 25.81, 24.88, 19.40, 16.50.

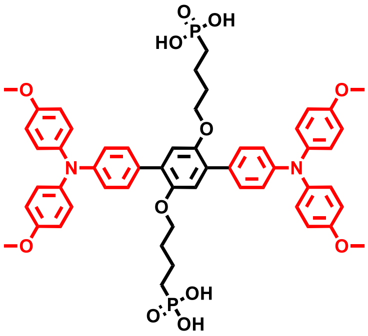

TDT

Synthesis of TDT.

TDT-P (1.32 g, 1.2 mmol) was dissolved in anhydrous dichloromethane (20 mL) under nitrogen atmosphere and trimethylbromosilane (4 mL) was added dropwise. Reaction was stirred for 18 h at room temperature. Afterwards solvent was partially distilled off under reduced pressure, and the liquid residue was dissolved in methanol (10 ml). Finally, distilled water was dropped slowly until a large amount of solid was produced. The solid was filtered off and washed with water to give a white solid of **TDT**. Yield: 1.09 g (91.8%). ^{1}H NMR (600 MHz, DMSO) δ = 7.43 (d, 4H), 7.06 (d, 8H), 6.94 (t, 10H), 6.81 (d, 4H), 3.93 (t, 4H), 3.75 (s, 12H), 1.71 (dd, 4H), 1.63 – 1.47 (m, 8H). ^{13}C NMR (151 MHz, DMSO) δ = 156.14, 140.63, 130.33, 127.10, 119.31, 115.52, 55.70, 55.37, 30.11, 19.93. ^{31}P NMR (243 MHz, DMSO) δ = 26.38. HRMS (ESI-TOF) m/z: $[M+Na]^+$ Calculated for $C_{54}H_{58}N_2O_{12}P_2$: 1011.98: Found: 1011.34.

Device fabrication.

Glass/ITO substrates were continuously washed in an ultrasonic bath for 15 min in detergent-deionized water solution, acetone and ethanol, respectively. The substrates were oven-dried and UV-treated for 30 minutes, then transferred into the N_2 glove box. D-SAM was dissolved in a mixed solvent of chloroform and methanol (1:1, v/v) at different concentrations. For HTLs, 0.2 mg mL^{-1} CDC was spin-coated on the substrate at 3000 rpm for 30 s, followed by annealing at 100 °C for 10 min; 0.2 mg mL^{-1} TDC was spin-coated on the substrate at 3000 rpm for 30 s, followed by annealing at 100 °C for 10 min; 0.1 mg mL^{-1} TDT was spin-coated on the substrate at 3000 rpm for 30 s, followed by annealing at 100 °C for 10 min. After that, the diluted Al_2O_3 dispersion solution (10 μL 20 wt.% Al_2O_3 solution in 1.7 mL IPA) was spin-coated on the HTL film at 5000 rpm for 30 s and annealed at 100 °C for 10 min. The Narrow bandgap (1.58 eV) perovskite $Cs_{0.05}FA_{0.75}MA_{0.2}Pb(I_{0.8}Br_{0.2})_3$ precursor solution was prepared by dissolving a mixture of 224.4 mg FAI, 16.2 mg MABr, 746.8 mg PbI_2, 12.7 mg MACl and 19.8 mg CsI in 1 mL DMF/DMSO (3:1, v/v) solution, and then magnetically stirring for several hours. The perovskite active layer was prepared by a one-step spin-coating method by spin-coating at 4000 rpm for 45 s. Before the end of spin-coating at 15 s, 200 μl of chlorobenzene was immediately dropped into the center of the substrate, followed by annealing at 65 °C for 5 min and then 105 °C for 20 min, covering the culture dish with a lid during the 65 °C annealing. Then 1.5 mg mL^{-1} of PEABr dissolved in IPA was spin-coated on the perovskite active layer at 5000 rpm for 30 s and annealed at 70 °C for 5 min. After that, 10 mg mL^{-1} of PCBM dissolved in chlorobenzene was spin-coated at 3000 rpm for 30 s. Lastly, complete devices were obtained by thermally evaporating 10 nm C_{60}, 8 nm BCP, and 100 nm Ag below 4×10^{-4} Pa, and evaporation rates at 0.1, 0.1-0.5, and 1 Å s^{-1}, respectively.

The Wide bandgap (1.68 eV) perovskite $Cs_{0.05}FA_{0.8}MA_{0.15}PbI_{2.25}Br_{0.75}$ precursor solution was prepared by dissolving a mixture of 192.6 mg FAI, 23.6 mg MABr, 131 mg $PbBr_2$, 536 mg PbI_2 and 18.2 mg CsI in 1 mL DMF/DMSO (4:1, v/v) solution, and then magnetically stirring for several hours. The perovskite active layer was prepared by a one-step spin-coating method by spin-coating at 4000 rpm for 45 s. Before the end of spin-coating at 15 s, 200 μl of chlorobenzene was immediately dropped into the center of the substrate, followed by annealing at 65 °C for 5 min and then 105 °C for 20 min, covering the culture dish with a lid during the 65 °C annealing.

Characterizations and measurements.

The ^{1}H NMR, ^{13}C NMR and ^{31}P NMR spectra were recorded on the Bruker (AVANCE III 600 MHz spectrometer). Thermogravimetric analysis (TGA) was based on an ARC accelerated calorimeter (STA4499F5, NETZSCH), N_2 atmosphere, 10 °C min^{-1}. Fourier transform infrared (FTIR) spectrograms were measured by Fourier transform infrared spectrometer (Nicolet IS10, America). Contact angle measurement was measured via a KRUSS Contact Angle Measuring Instrument (DSA100). The transmittance of D-SAM films and the absorbance of perovskite films was measured using a Shimadzu UV-2600i spectrophotometer. Ultraviolet photoelectron spectroscopy (UPS) spectra were obtained using a non-monochromated He I photon source (hν = 21.22 eV). The X-ray photoelectron spectroscopy (XPS) spectra was determined using a monochromatic Al-Ka (1486.6 eV) radiation source (Thermo Fisher Scientific). The XRD patterns were obtained by an X-ray diffractometer (Bruker D8 Discover) with Cu Kα radiation (λ = 1.5418 Å) at 40 kV and 30 mA. KPFM and AFM was measured with Nanosurf AG, Flex-Mount Atomic Force Microscope. SEM-EDS was recorded by Thermo Scientific Apreo 2C, OXFORD ULTIM Max65 operated at 5 kV. The photoluminescence (PL) Spectroscopy and PL mapping were characterized using a WITec Alpha 300R Raman fluorescence spectrometer with an excitation wavelength of 532 nm. Time resolved photoluminescence (TRPL) were conducted with FLS-1000 fluorescence spectrometer. The femtosecond transient absorption spectrum (TA) was characterized by Dalian Chuanrui TA100. Transient photovoltage (TPV) and transient photocurrent (TPC) measurements and Mott-Schottky were tested in the dark using an electrochemical workstation (Paios), at room temperature with 40 % humidity. *J-V* curves were measured in a nitrogen-filled glove box using a standard xenon solar simulator (LSS-55) to simulate AM 1.5G irradiation (100 mW cm^{-2}), with light intensity calibrated using a silicon reference cell (LRC-KG2-008) before measurement. The active area of the device is 0.08 cm^2 and the device is no preconditioning before measurement. The EQE spectra were measured under ambient conditions with a quantum efficiency measurement system (model LST-QE). The electrochemical impedance spectroscopy (EIS) measurements were obtained from a biologic vsp-3e electrochemical workstation. The test temperature was 300 K and the magnetic field strength was either 0.5 T or 1 T. Dark *J-V* curves of the devices to evaluate the hole transport ability were measured in the range of (-2) - (+2) V. Both SCLC and Dark *J-V* curves are measured in a dark field environment using the same instruments (standard xenon solar simulator, LSS-55) as *J-V* curve testing. Space-charge limited current (SCLC) measurement based on the hole only devices (ITO/Me-4PACz/perovskite with or without dopant/Sprio-OMeTAD/Ag) were measured in the range of 0-8 V.

Calculation procedures

Supplementary Note S1. First-principles Calculations.

Vienna *ab* initio Simulation Package (VASP) code was employed to implement the first-principles calculations for all the DFT simulations in this work.[1] We use projector augmented-wave (PAW) pseudopotentials with a plane-wave energy cutoff of 450 eV.[2] The exchange-correlation energy was treated by employing the Perdew-Burke-Ernzerhof (PBE) formulation of generalized gradient approximation (GGA).[3] We set the energy convergence criterion as 1×10^{-5} eV. The force convergence criterion for structure relaxation is set to less than 0.02 eV/Å. A Γ-centered 2×2×1 k-point grids was set to sample the Brillouin zone.

After the bulk In_2O_3 was fully optimized, it was cleaved along the (111) plane, resulting in surfaces terminated with indium (In) and oxygen (O). Subsequently, an 80-atom supercell was created by expanding the In_2O_3 (111) plane using the transformation matrix:

$$\begin{bmatrix} 1 & 0 & 0 \\ 1 & 2 & 0 \\ 0 & 0 & 1 \end{bmatrix}.$$

To eliminate interactions between periodic images, a vacuum interval of 20 Å was introduced. Then, the molecules of CDC, TDC and TDT was added on the In_2O_3 (111) to construct the In_2O_3 (111)-CDC, In_2O_3 (111)-TDC, In_2O_3 (111)-TDT structures, respectively.

The adsorption energies in this work were calculated according to the formula.

$$E_{ads} = E_s - E_{slab} - E_{molecule}$$

Here, E_s denotes the total energy of the system. E_{slab} is the energy of In_2O_3 (111) surface. $E_{molecule}$ represents the energy of molecule (CDC, TDC and TDT).[4,5] The charge transfer between In_2O_3 (111) surface and the molecules of CDC, TDC and TDT are investigated by the charge difference analysis.[6,7]

Supplementary Note S2. Ideality factor and FF_{max} calculations.

The V_{OC} of PSCs is measured under a range of light intensities (Plight) and plotted as a function of Plight in logarithm scales, and the ideality factor (n) is obtained according to the following formula:[8]

$$V_{oc} = n\frac{kT}{q}\ln I + C$$

The FF loss between Shockley-Queisser (S-Q) limit value of FF and the FF measurement value consists of non-radiative recombination loss and charge transport loss. The FF maximum value ($\mathrm{FF_{max}}$) without charge transport loss can be determined by the following equation:[9,10]

$$FF_{max} = \frac{V_{oc} - \ln(V_{oc} + 0.72)}{V_{oc} + 1}$$

where q, K, I, and T are the charge of an electron, the Boltzmann constant, light intensity, and the temperature, respectively.

Supplementary Note S3. $\mathrm{V_{bi}}$ calculations.

The V_{bi} can be obtained from the Mott-Schottky curve:

$$\frac{1}{C^2} = \frac{2(V_{bi} - V)}{A^2 q\varepsilon\varepsilon_0 N_d}$$

Where ε is the vacuum permittivity and ε_0 is the relative dielectric constant of the perovskite material.[11]

Supplementary Note S4. QFLS calculations.

Calculate the quasi-Fermi energy level splitting of the internal electron-hole using the equation:[12,13]

$$QFLS = k_B T\ln(PLQY\frac{J_G}{J_{0,rad}})$$

where k_B is Boltzmann's constant, T is the temperature (300K), J_G is the current density generated in illumination, and $J_{0,rad}$ is the dark radiative recombination current density. We approximate the short-circuit current density of the solar cell to obtain J_G. $J_{0,rad}$ is calculated by the following equation:

$$J_{0,rad} = q\int EQE_{pv}(E)\Phi_{BB}(E)dE$$

where q is the elementary charge, EQE_{PV} is the photovoltaic external quantum efficiency, and ϕ_{BB} is the blackbody photon flux:

$$\Phi_{BB}(E) = \frac{2\pi E^2}{h^3c^2}\exp\left(\frac{-E}{k_B T}\right)$$

where E, h and c are photon energy, plank's constant and the speed of light in a vacuum, respectively.

Supplementary Note S5. n_{trap} calculations.

The SCLC curves were based on the electron-only devices. The trap density (n_{trap}) is determined by the trap-filled limit voltage (V_{TFL}) based on the following equation:[14]

$$n_{trap} = \frac{2V_{TFL}}{qL^2}\varepsilon_r\varepsilon_0$$

Where L is the thickness of the perovskite film, V_{TFL} is the onset voltage of the trap-filled limit region, ε_r is the relative dielectric constant of perovskite film, ε_0 is the vacuum permittivity, and q is the electron charge.

Figures and Tables.

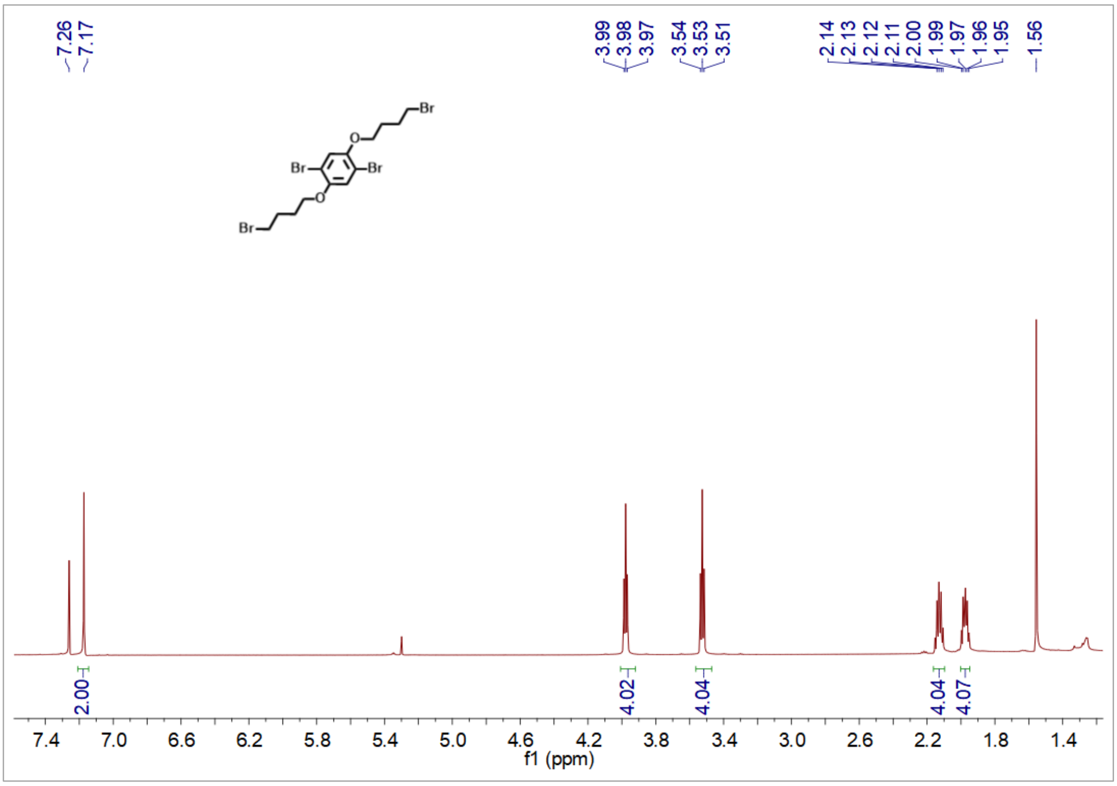

Figure S1. The ^{1}H NMR spectrum of **D1** in $CDCl_3$.

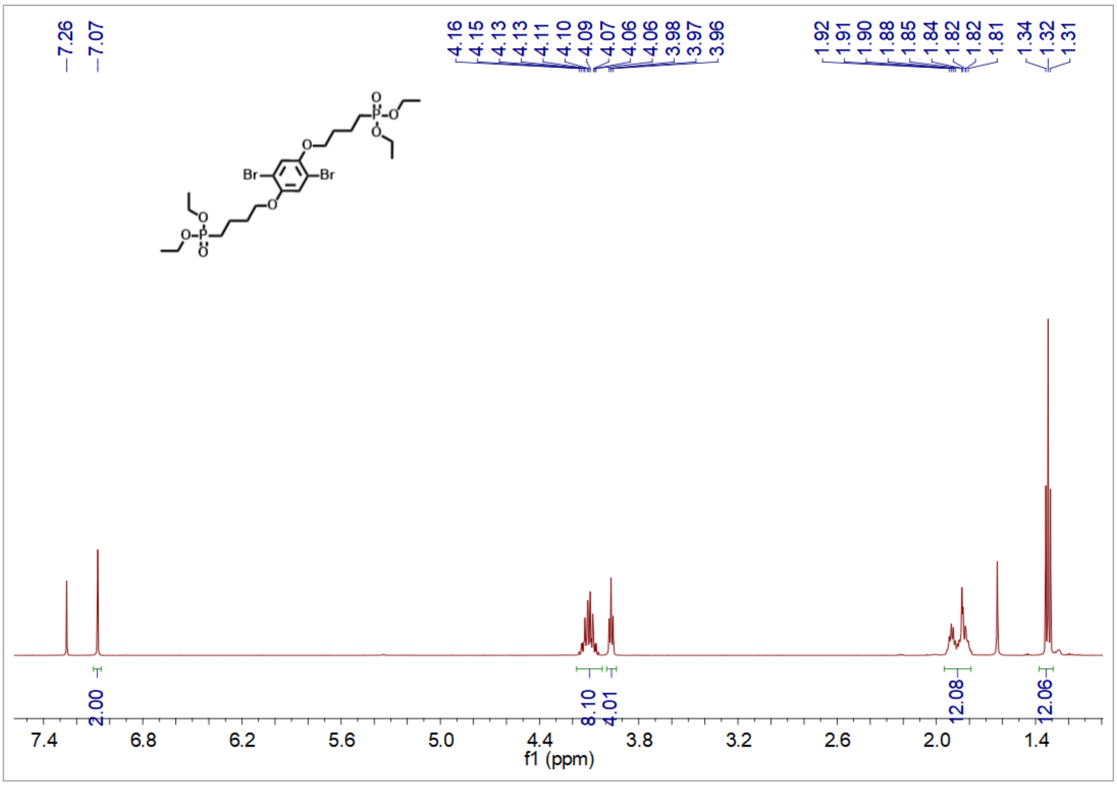

Figure S2. The ^{1}H NMR spectrum of **D2** in $CDCl_3$.

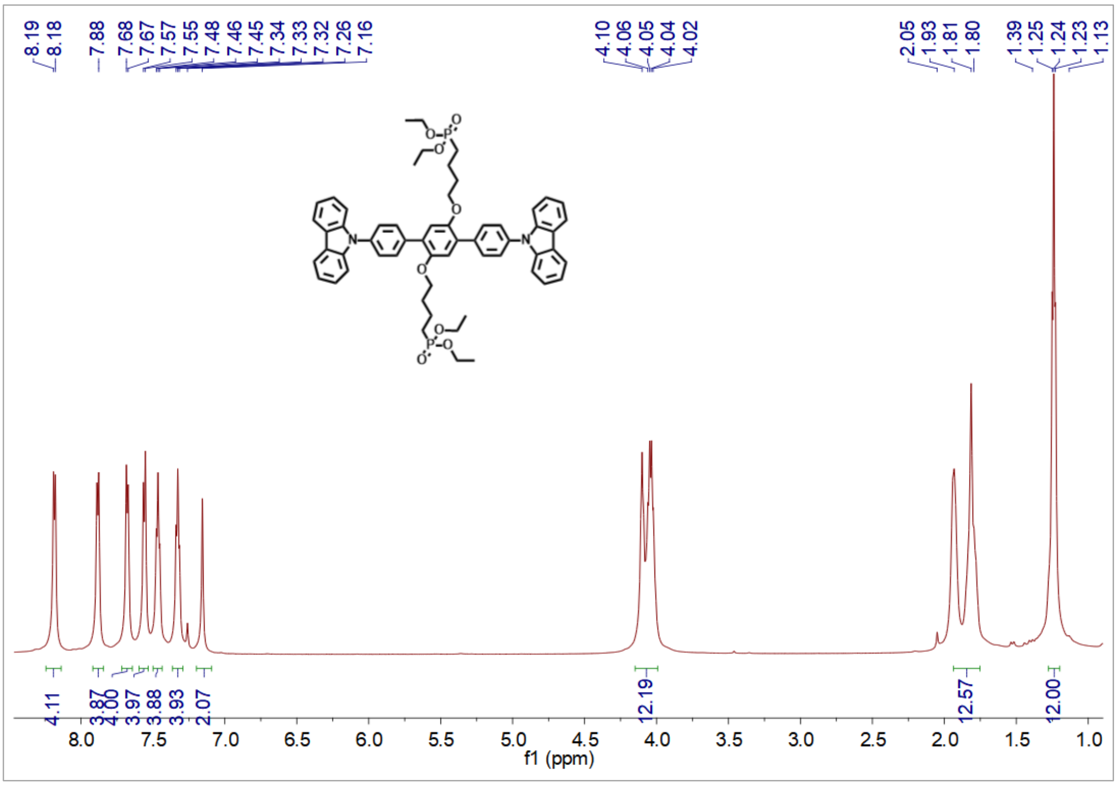

Figure S3. The ^{1}H NMR spectrum of **CDC-P** in $CDCl_3$.

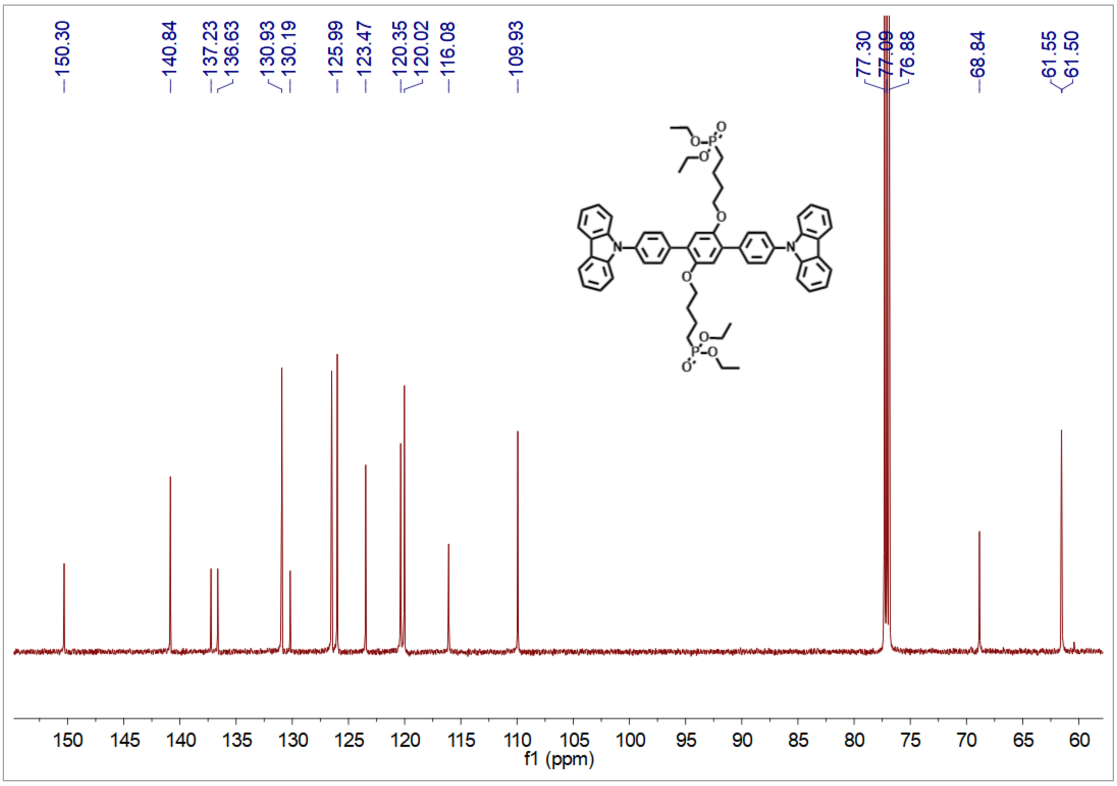

Figure S4. The ^{13}C NMR spectrum of **CDC-P** in $CDCl_3$.

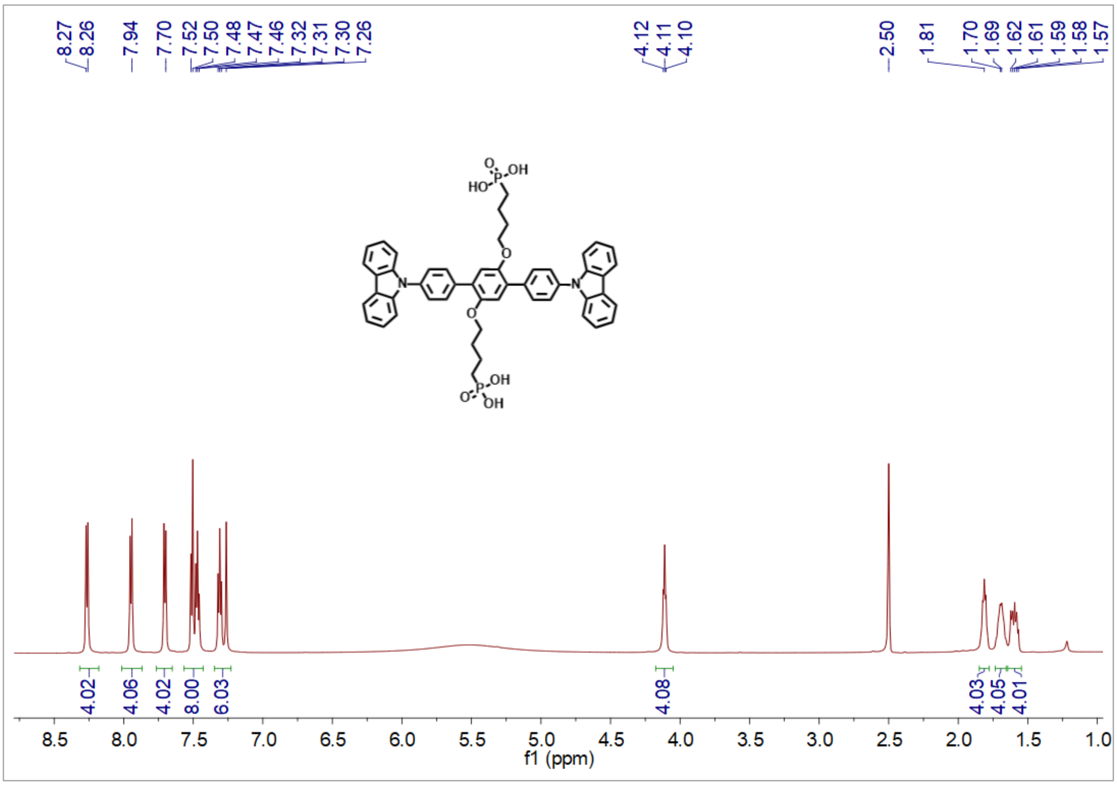

Figure S5. The ^{1}H NMR spectrum of **CDC** in DMSO-d_6.

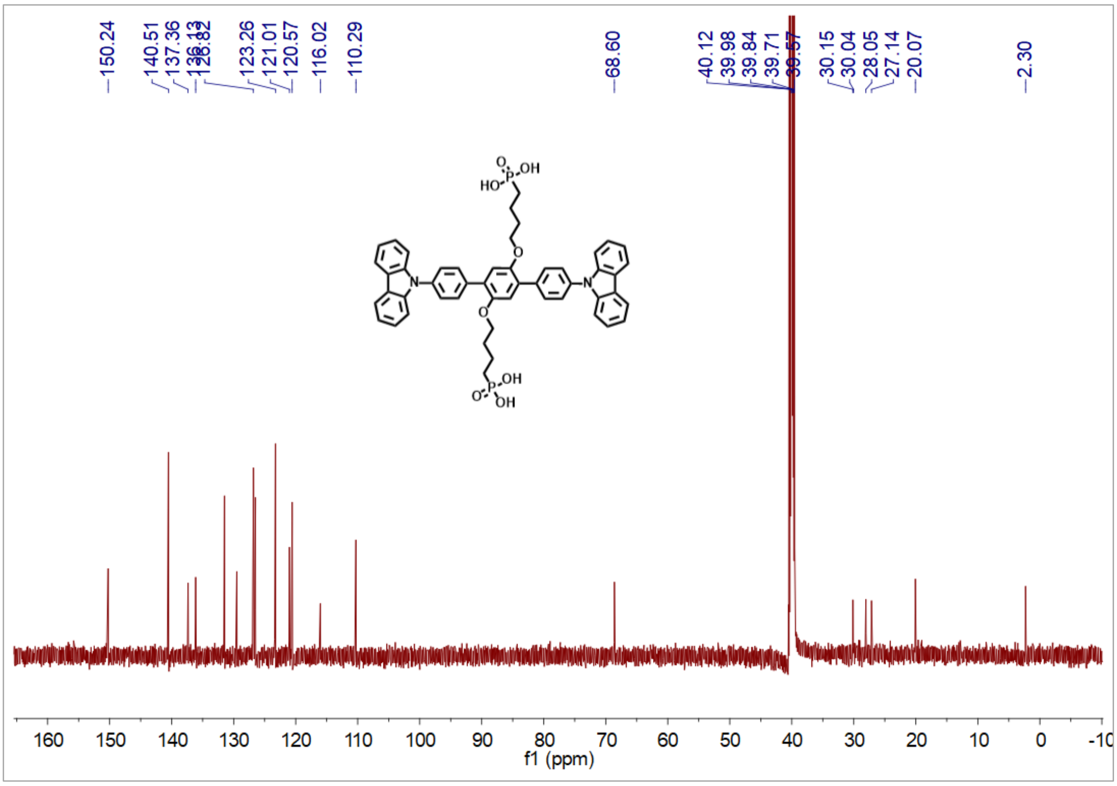

Figure S6. The ^{13}C NMR spectrum of **CDC** in DMSO-d_6.

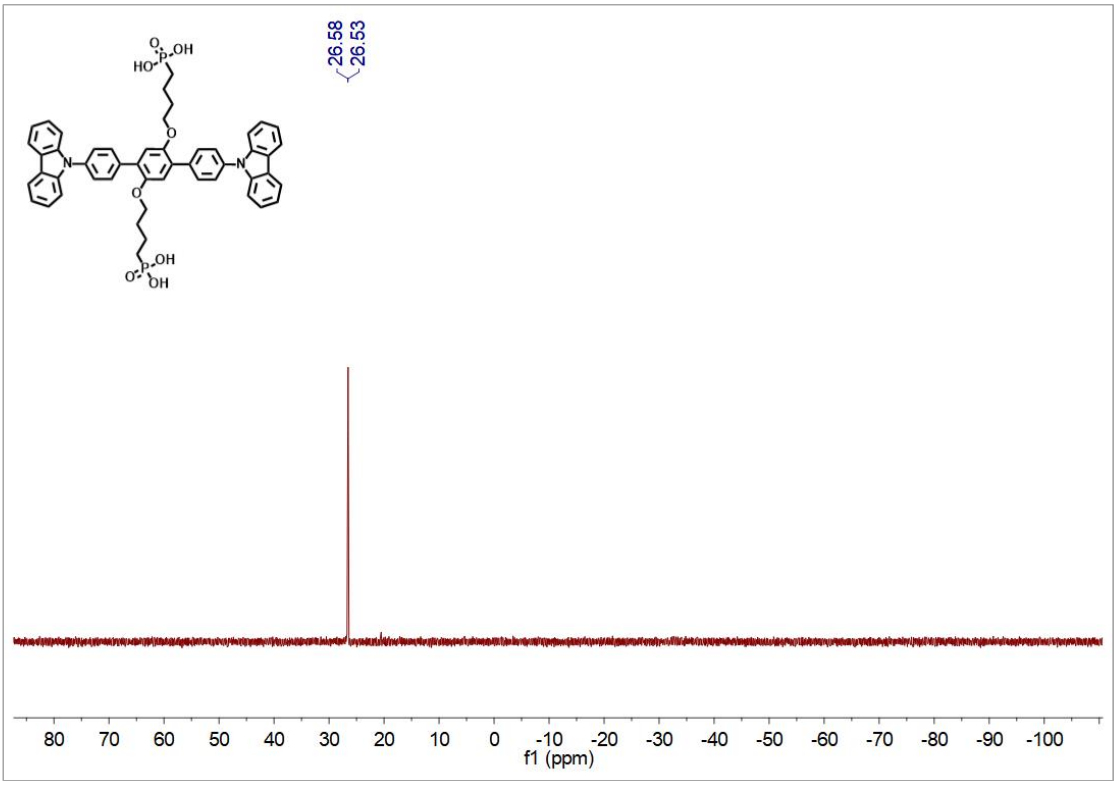

Figure S7. The ^{31}P NMR spectrum of **CDC** in DMSO-d_6.

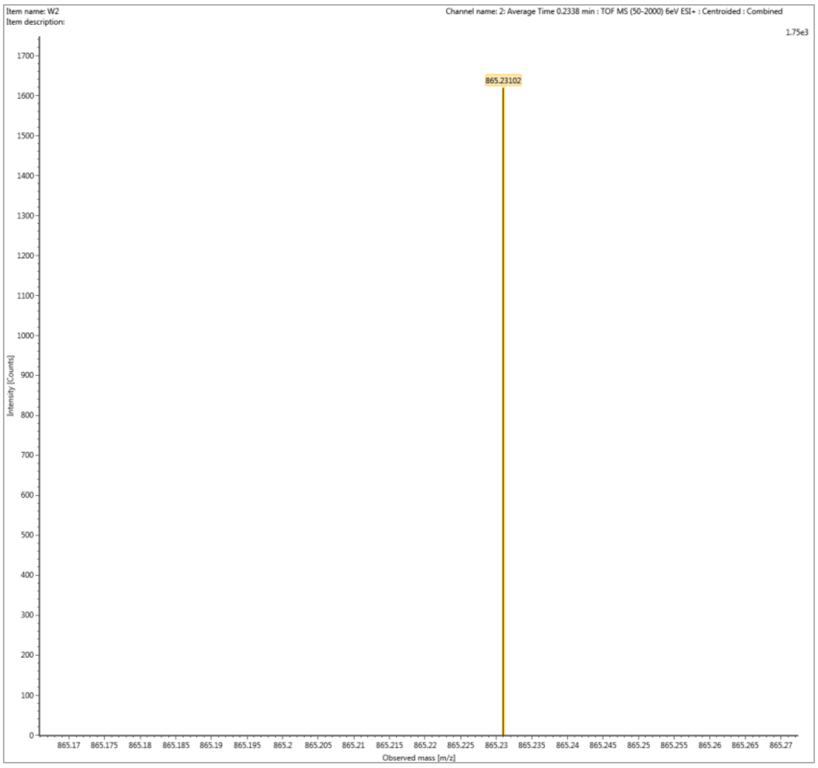

Figure S8. The mass spectrometry of **CDC**.

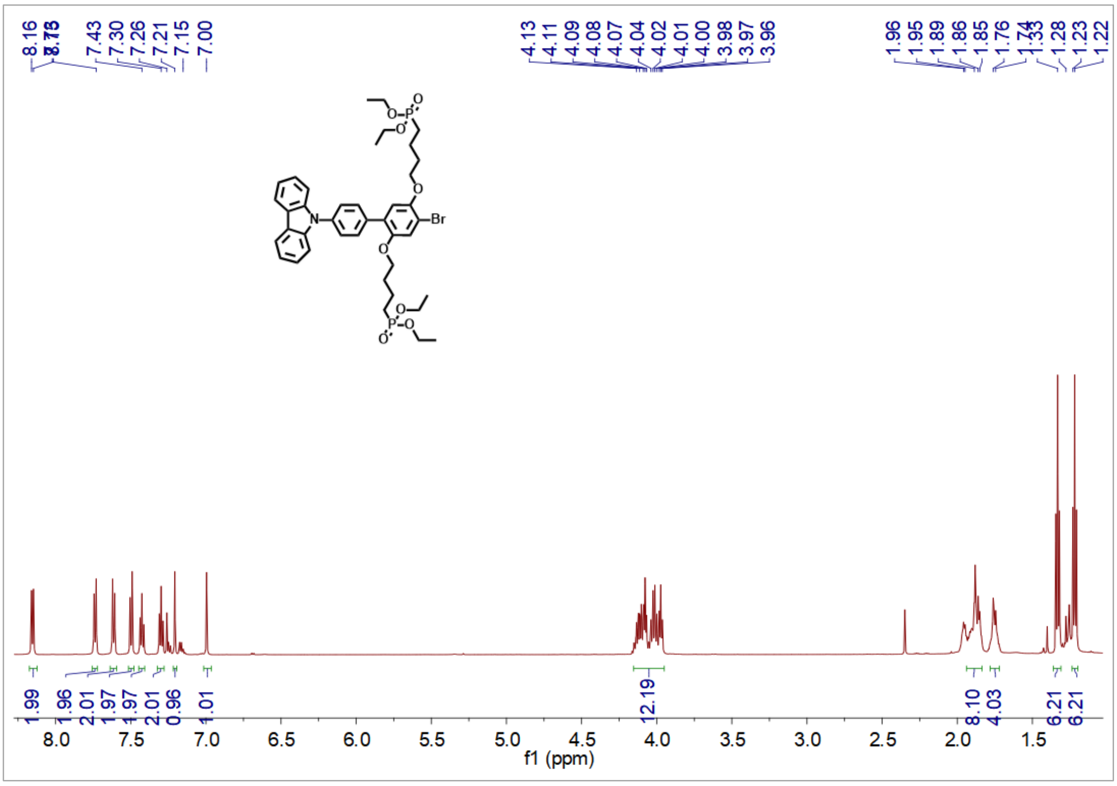

Figure S9. The ^{1}H NMR spectrum of **CD-P** in $CDCl_3$.

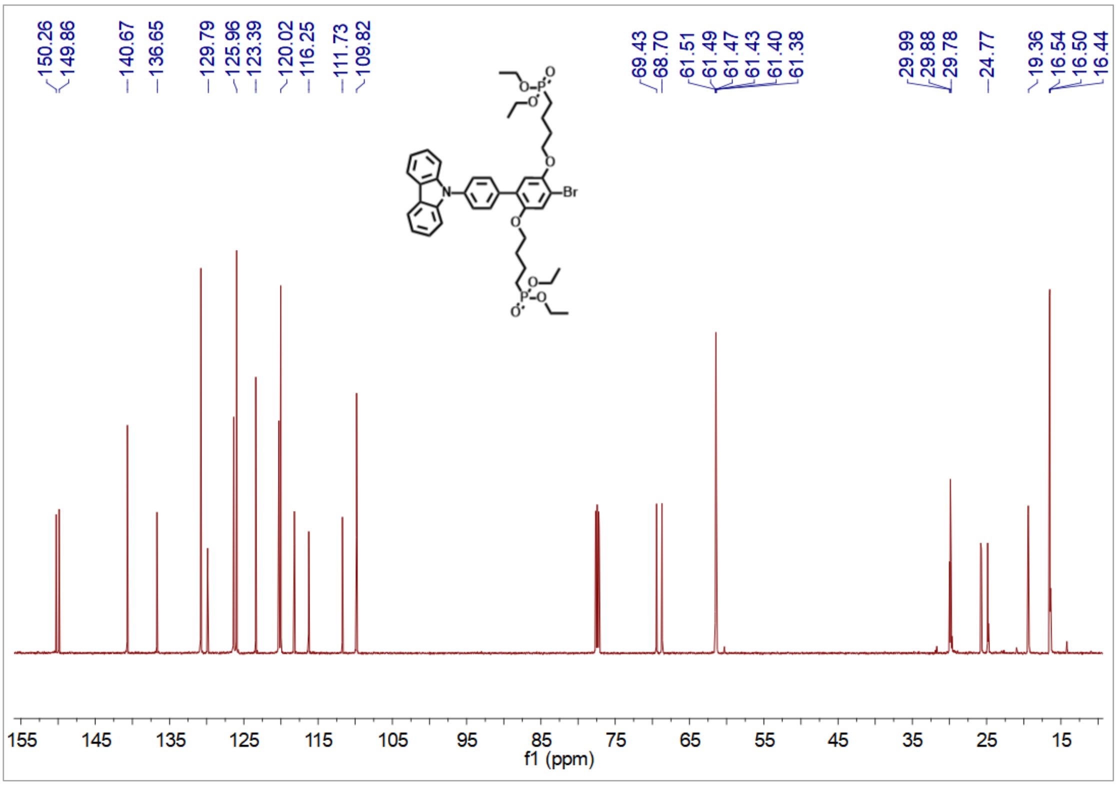

Figure S10. The ^{13}C NMR spectrum of **CD-P** in $CDCl_3$.

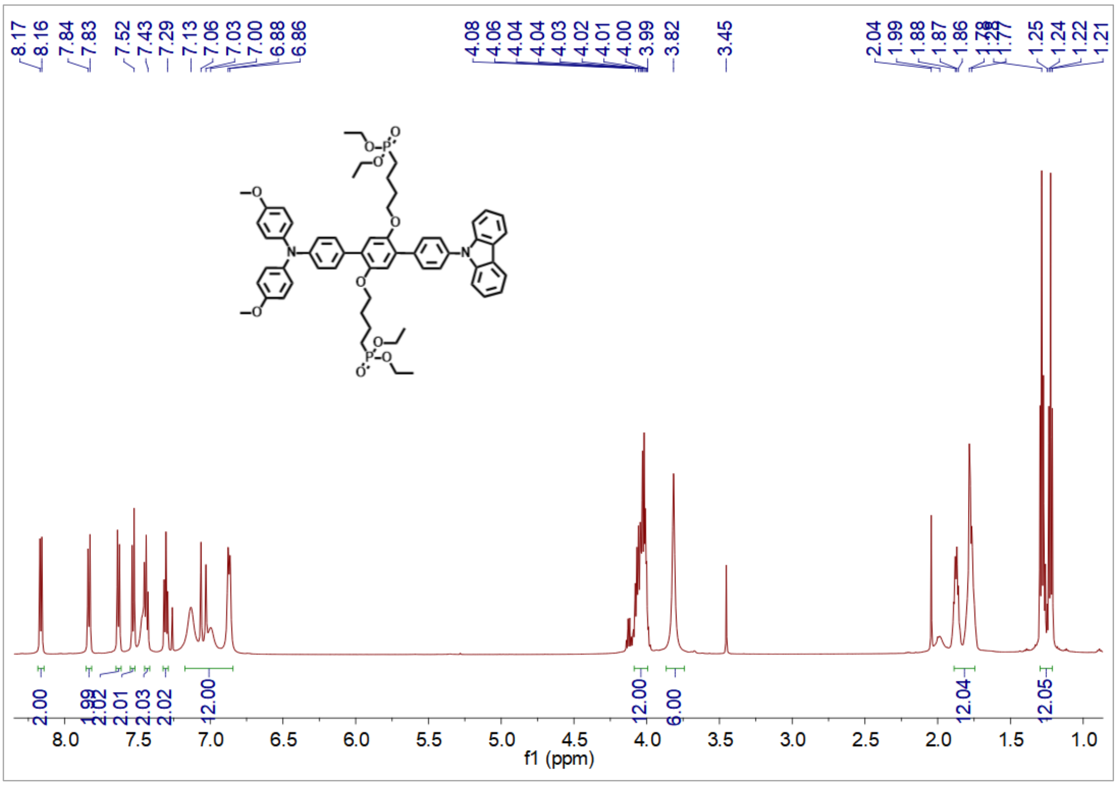

Figure S11. The ^{1}H NMR spectrum of **TDC-P** in $CDCl_3$.

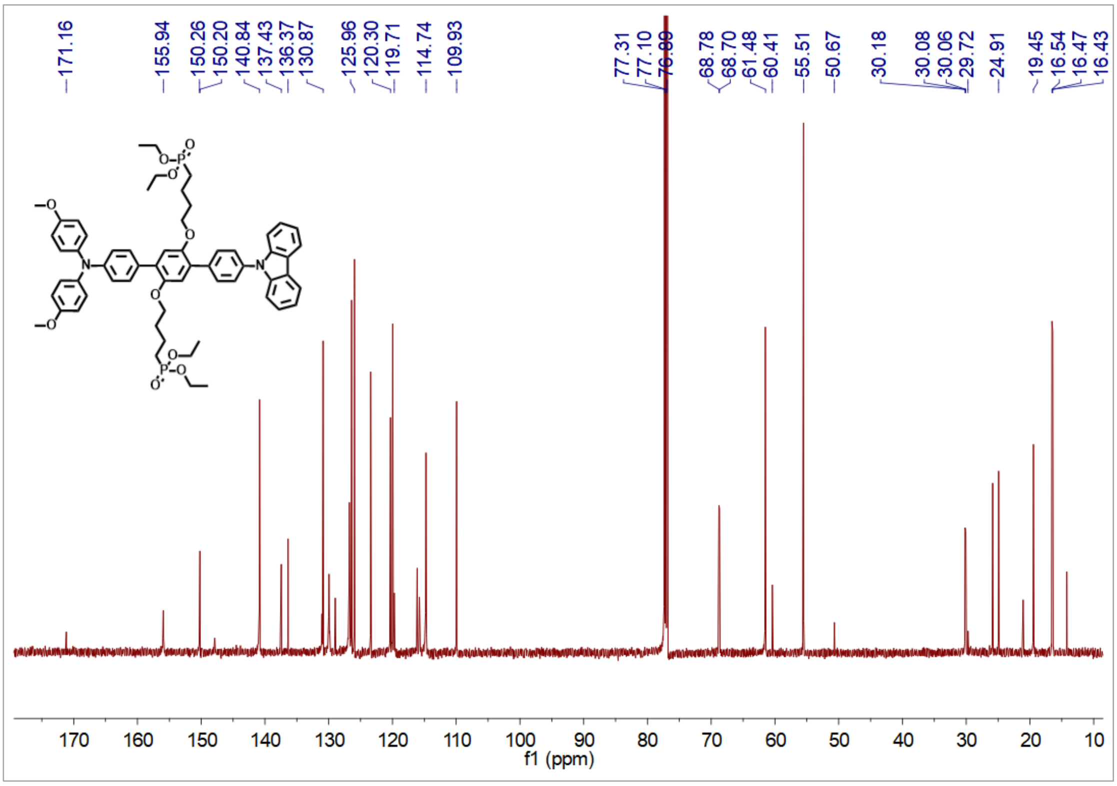

Figure S12. The ^{13}C NMR spectrum of **TDC-P** in $CDCl_3$.

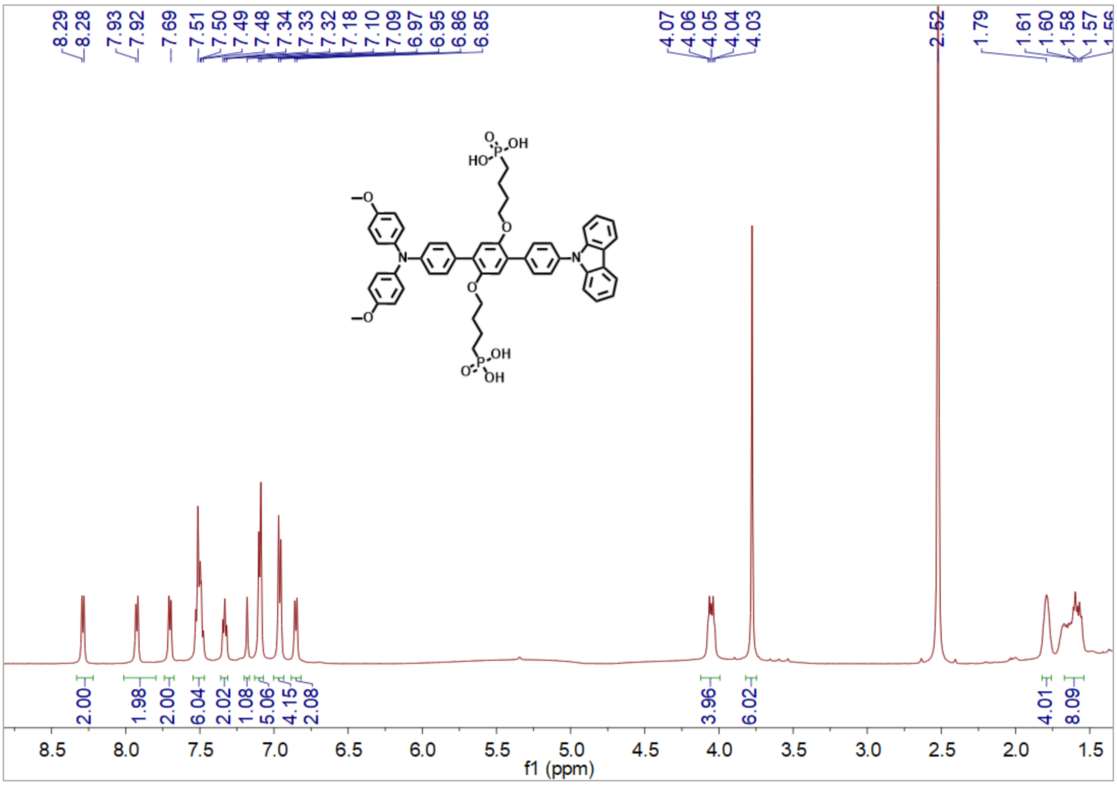

Figure S13. The ^{1}H NMR spectrum of **TDC** in DMSO-d_6.

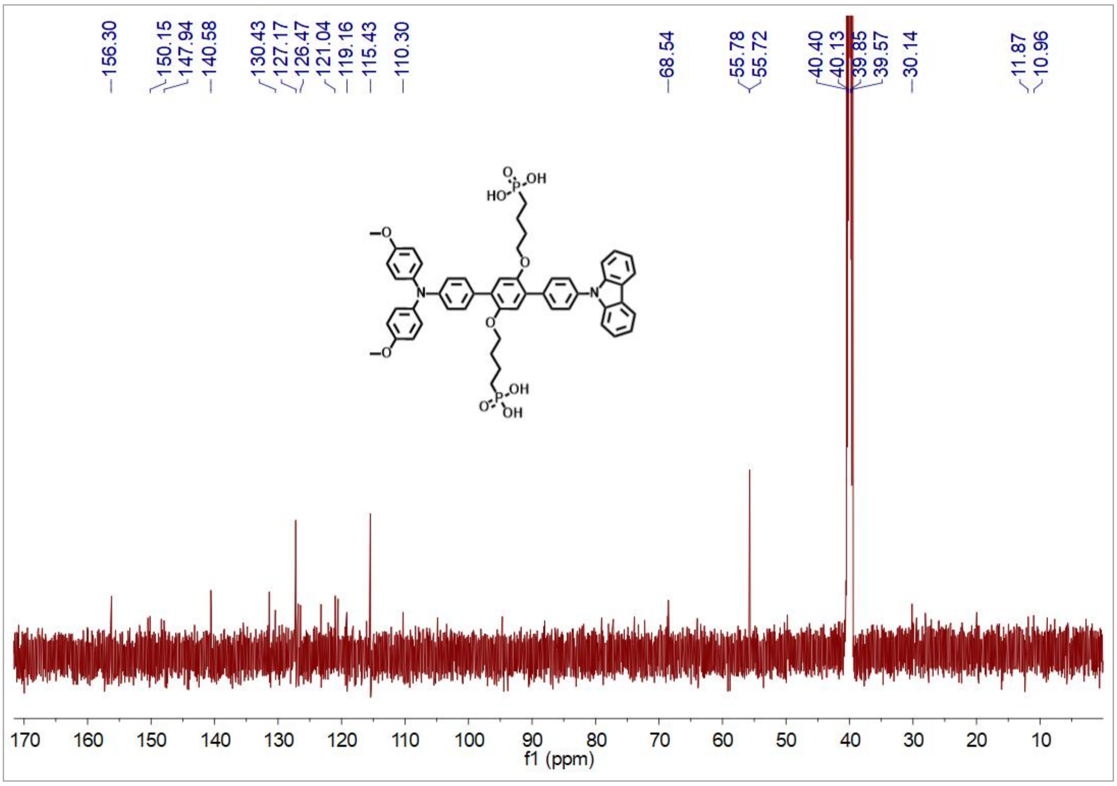

Figure S14. The ^{13}C NMR spectrum of **TDC** in DMSO-d_6.

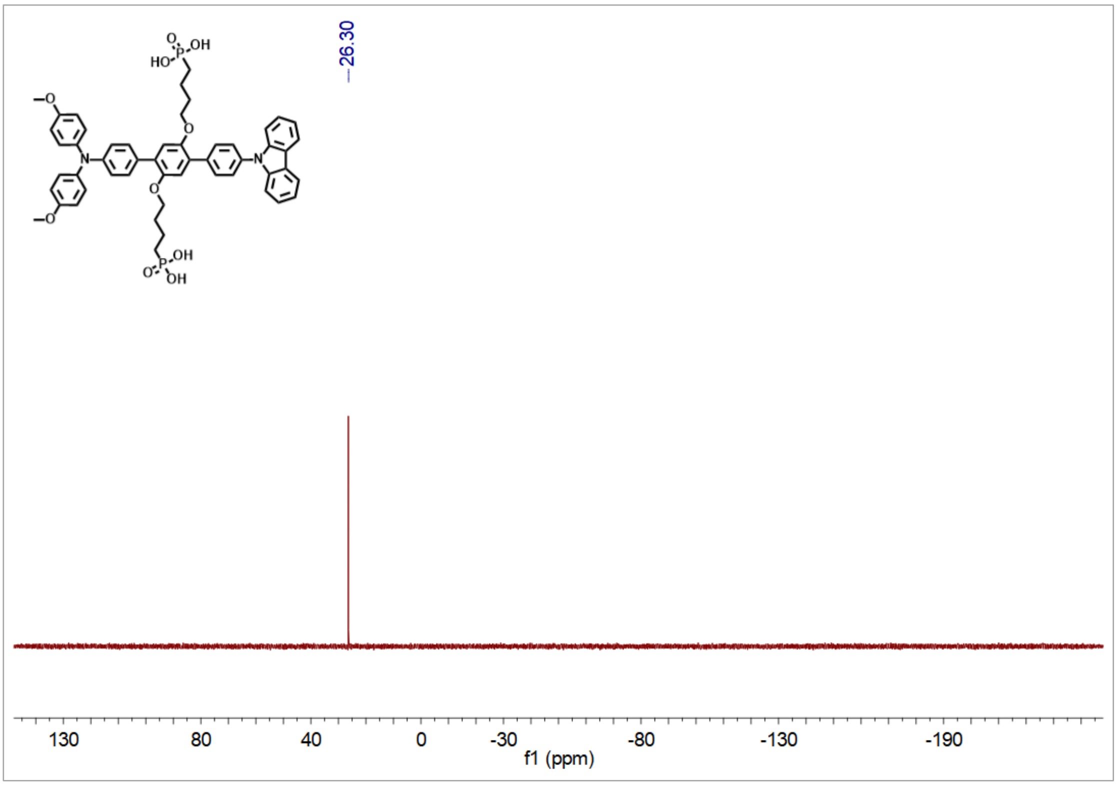

Figure S15. The ^{31}P NMR spectrum of **TDC** in DMSO-d_6.

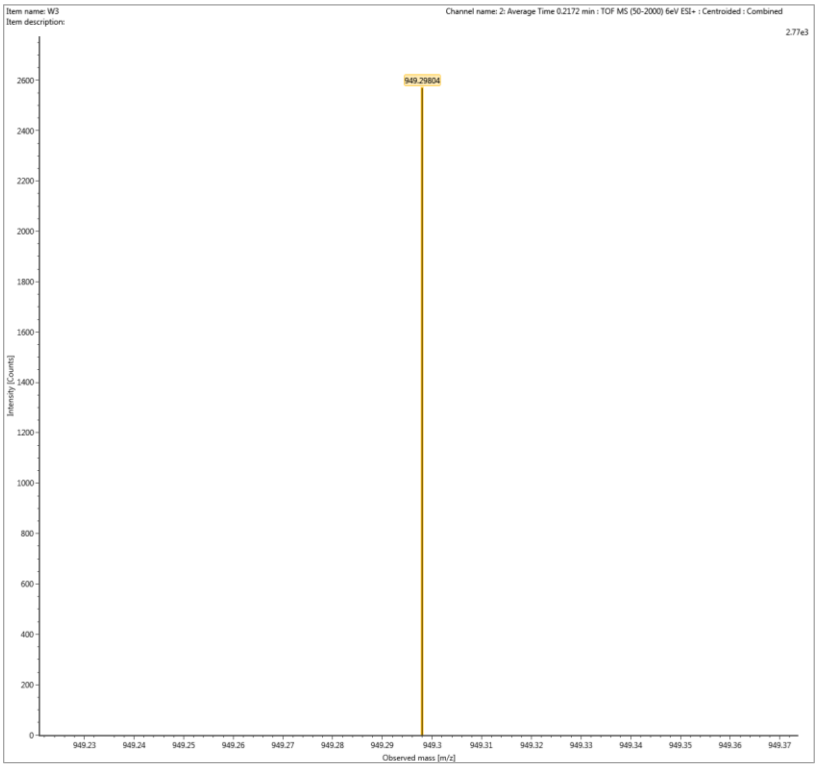

Figure S16. The mass spectrometry of **TDC**.

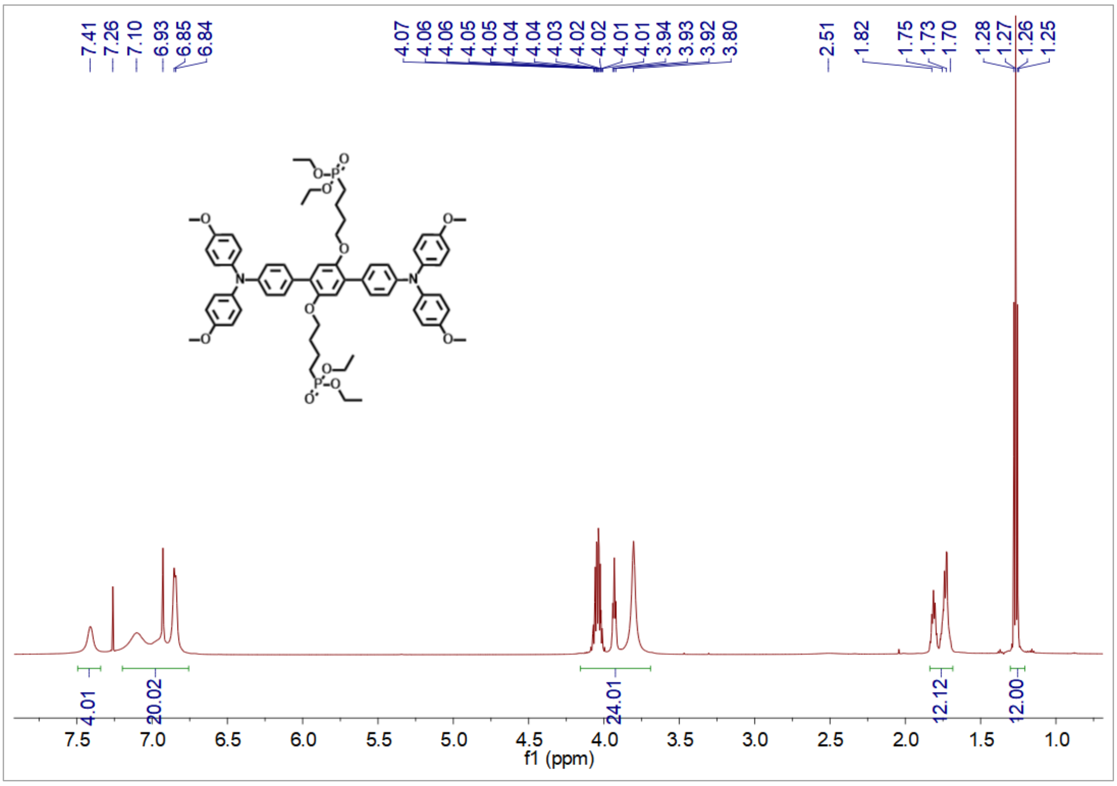

Figure S17. The ^{1}H NMR spectrum of **TDT-P** in $CDCl_3$.

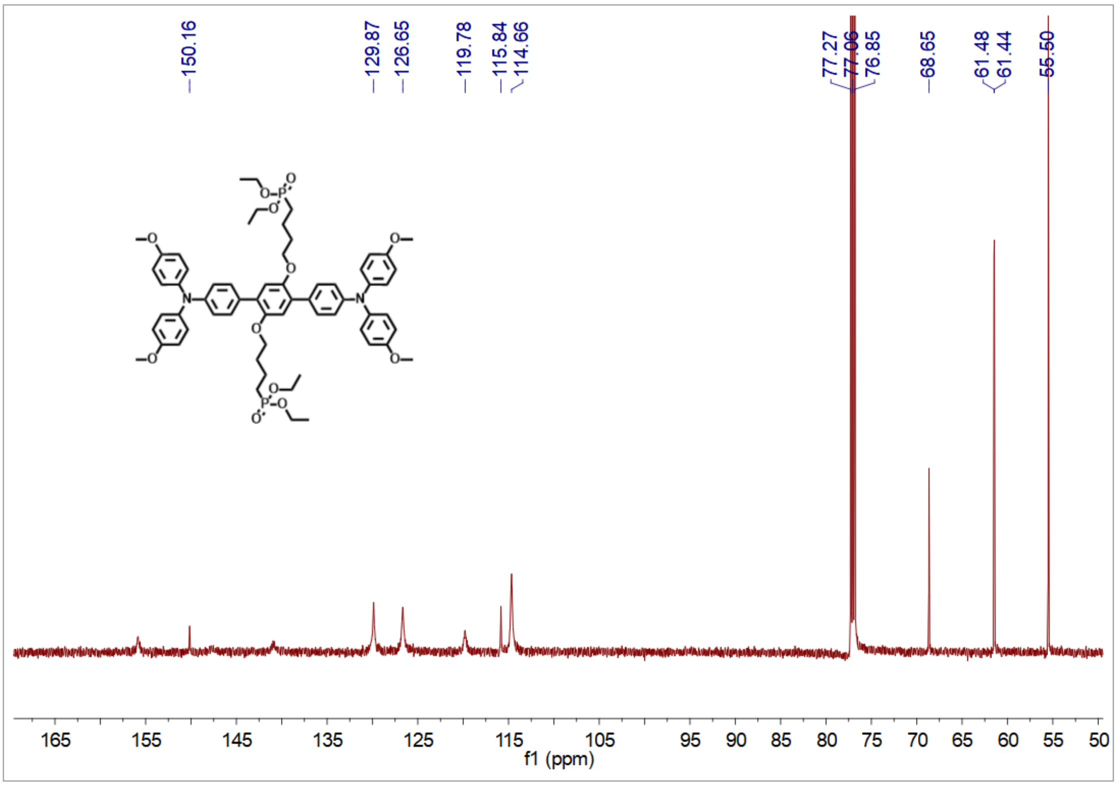

Figure S18. The ^{13}C NMR spectrum of **TDT-P** in $CDCl_3$.

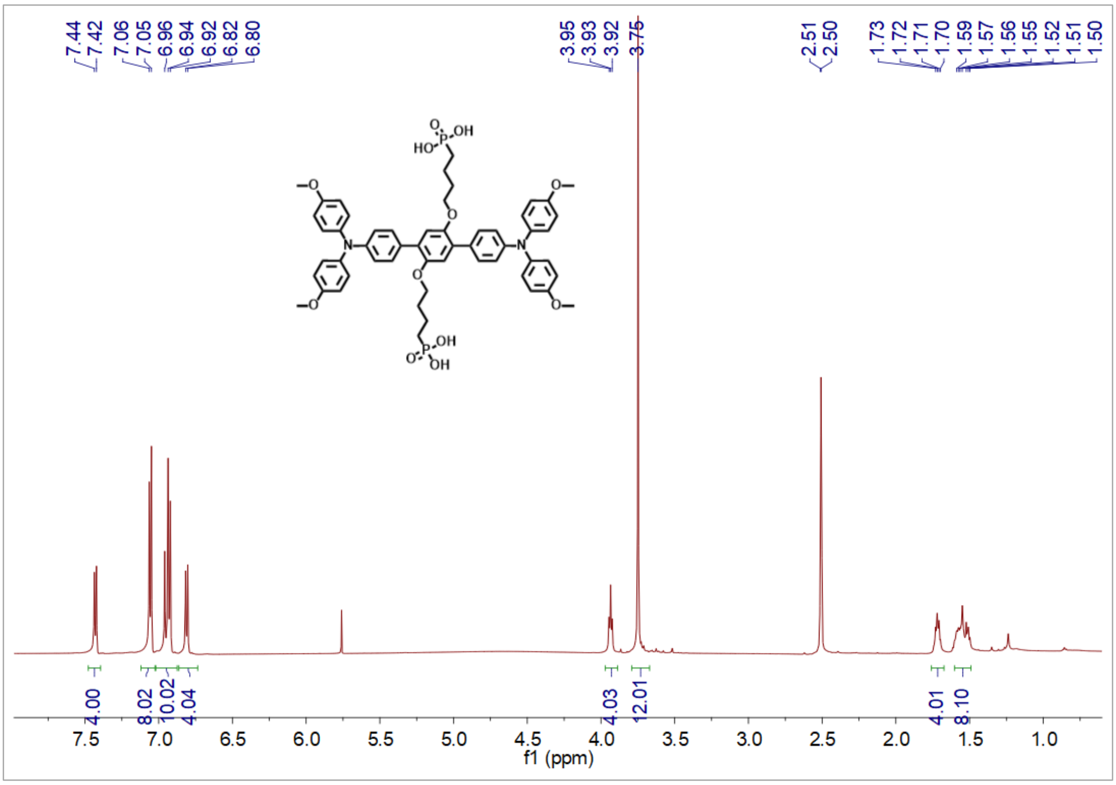

Figure S19. The ^{1}H NMR spectrum of **TDT** in DMSO-*d*$_6$.

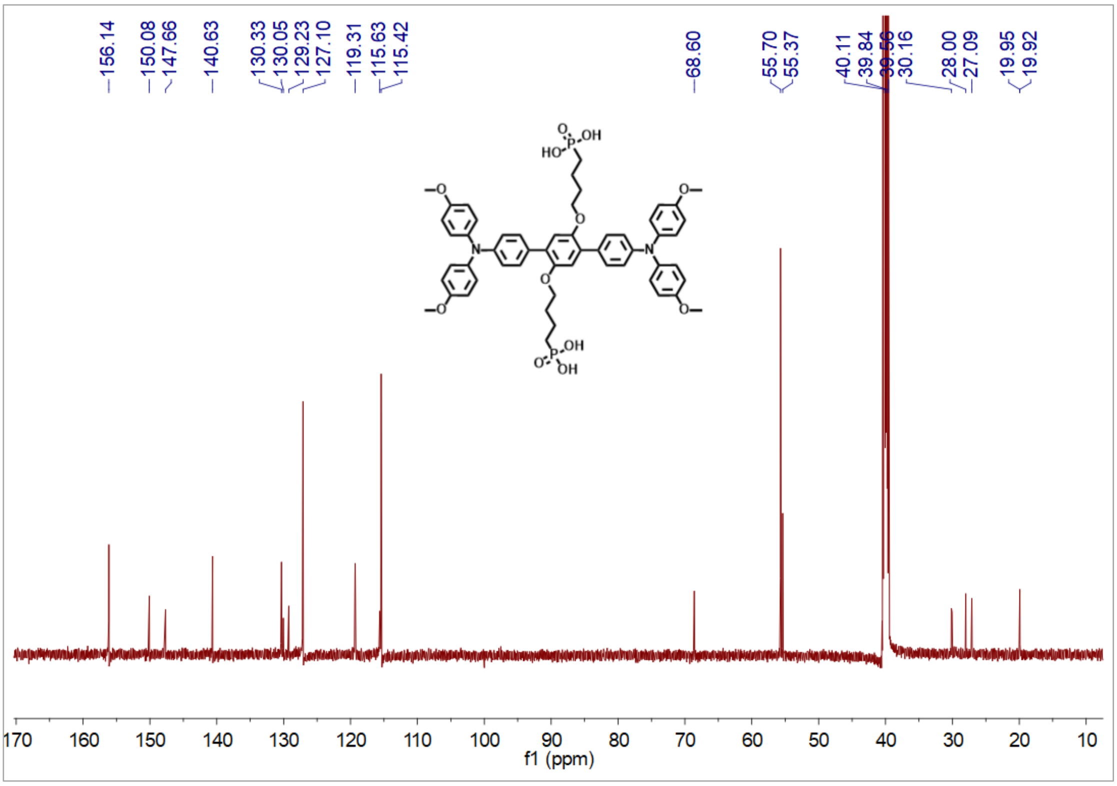

Figure S20. The ^{13}C NMR spectrum of **TDT** in DMSO-*d*$_6$.

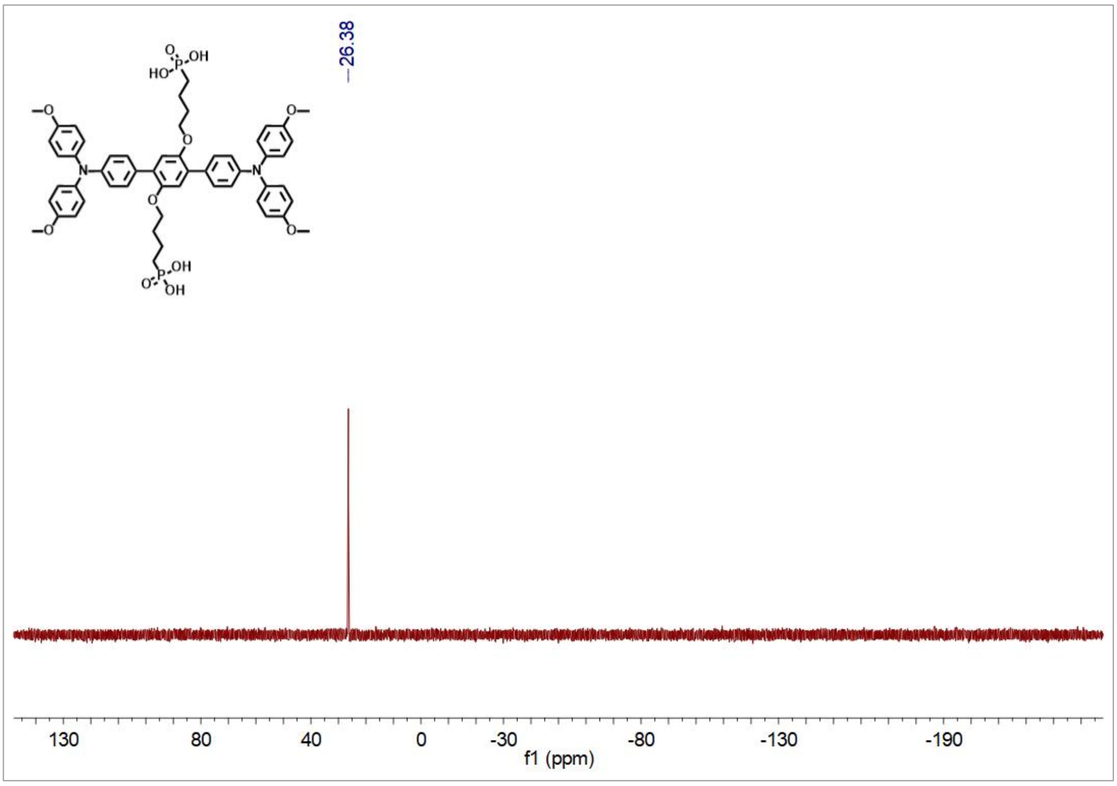

Figure S21. The ^{31}P NMR spectrum of **TDT** in DMSO-d_6.

Figure S22. The mass spectrometry of **TDT**.

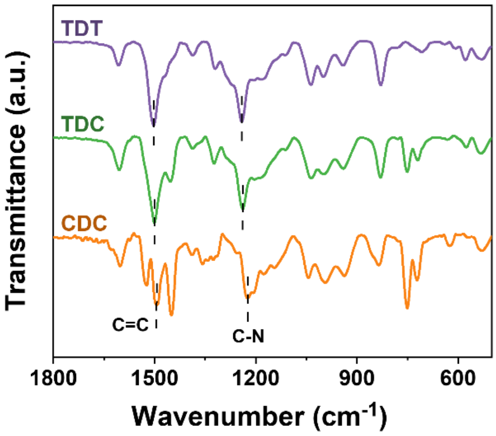

Figure S23. The FTIR spectrum of the CDC, TDC and TDT dispersed in KBr solid.

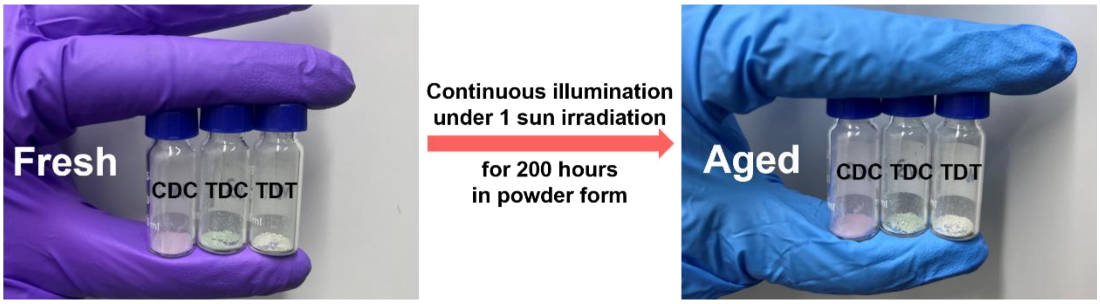

Figure S24. The photographs of fresh and aged SAMs under continuous 1 sun irradiation for 200 hours in powder form.

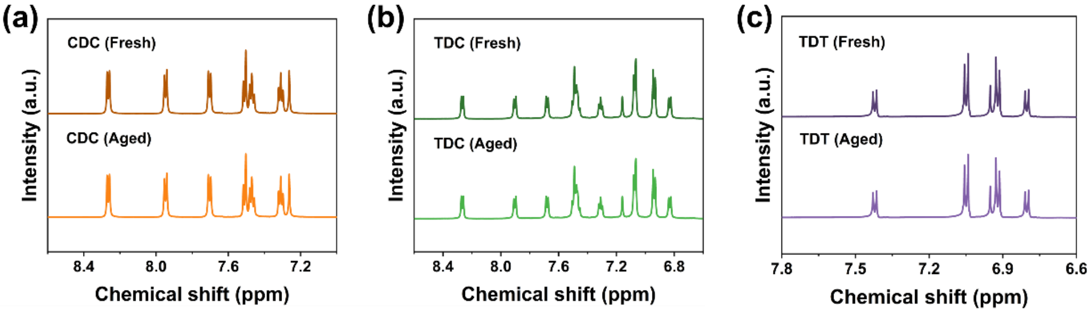

Figure S25. ^{1}H NMR spectra (low field region) of fresh and light-aged D-SAMs in DMSO-d6.

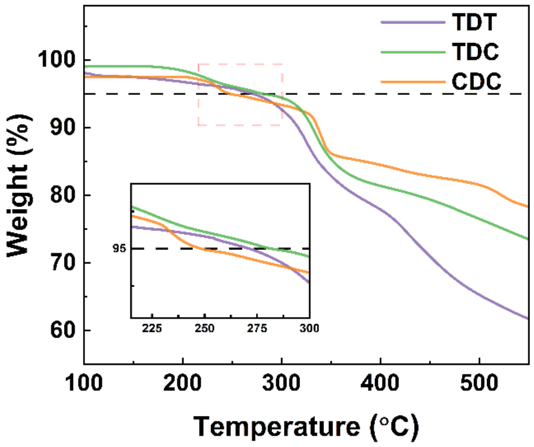

Figure S26. Thermogravimetric analysis curves of CDC, TDC and CDC.

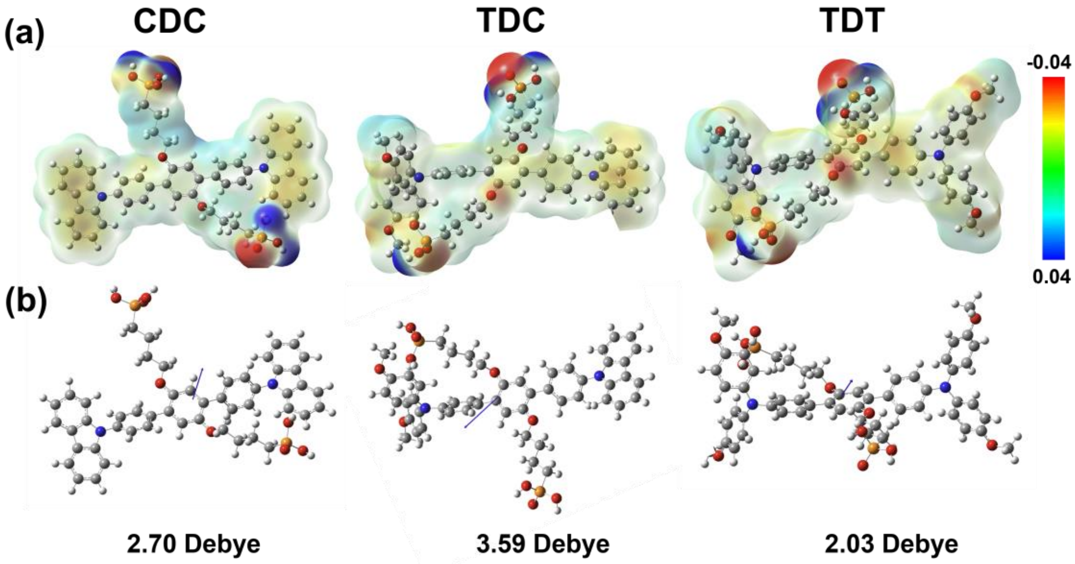

Figure S27. (a) The electrostatic potential and (b) dipole moment of CDC, TDC and CDC.

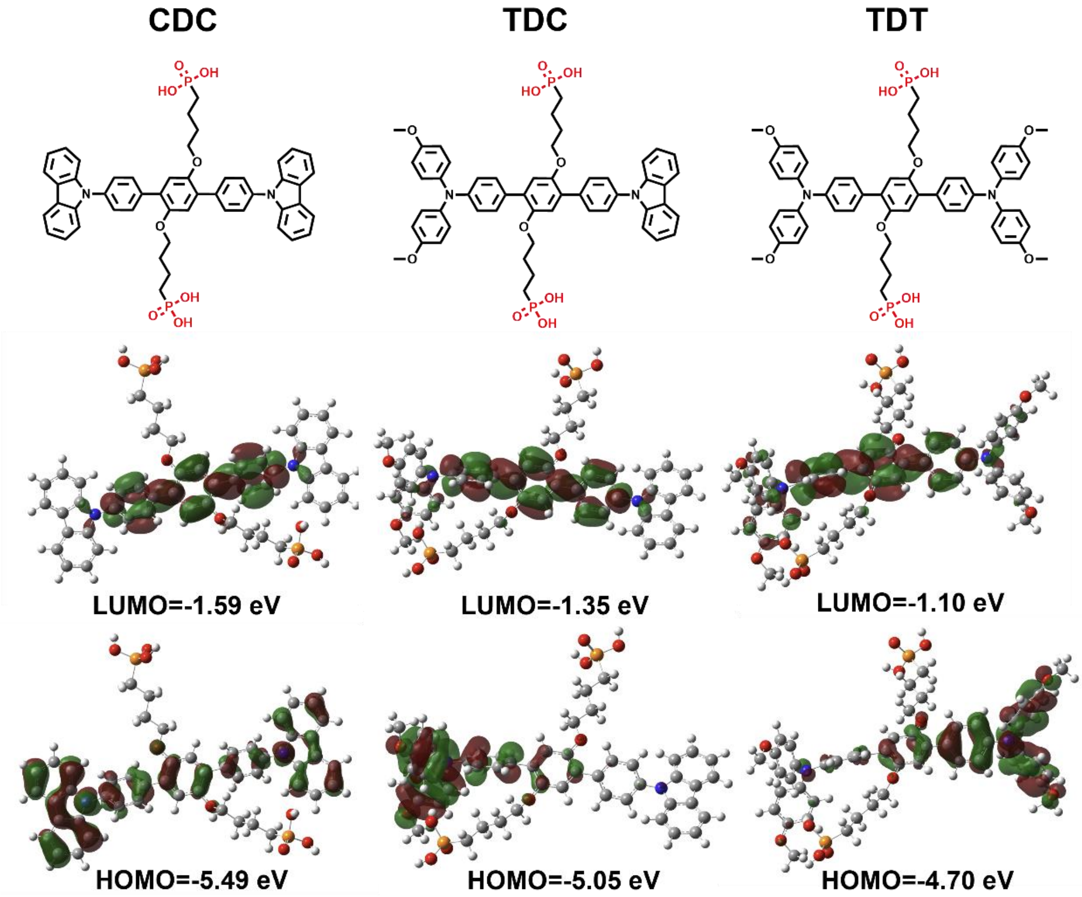

Figure S28. The calculated LUMO/HOMO orbitals and energy levels of D-SAMs. The dipole moments, and molecular orbitals energy levels were calculated by density functional theory (DFT) at the level of the B3LYP /6-311G(d,p) basis set with Gaussian09 package.

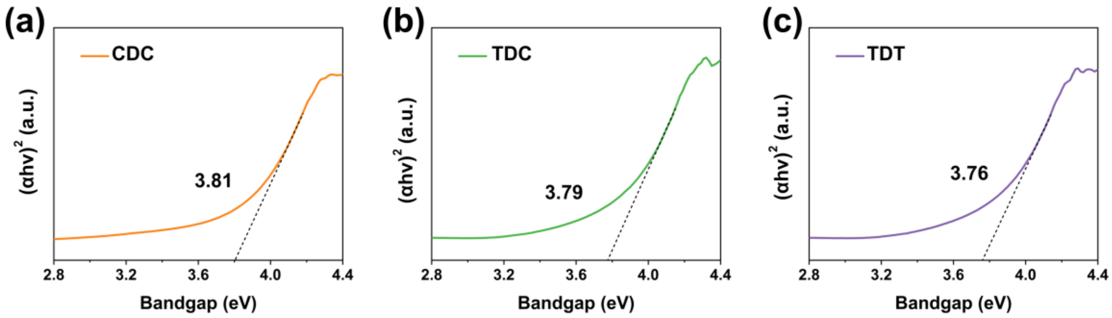

Figure S29. Tauc-plot curves of ITO/CDC, ITO/TDC and ITO/TDT substrates.

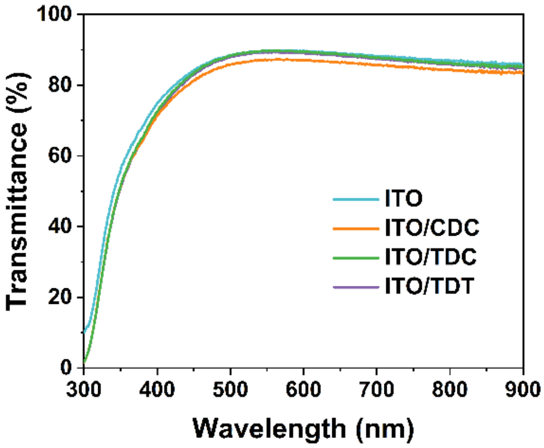

Figure S30. The high transmittance of ITO, ITO/CDC, ITO/TDC and ITO/TDT substrates.

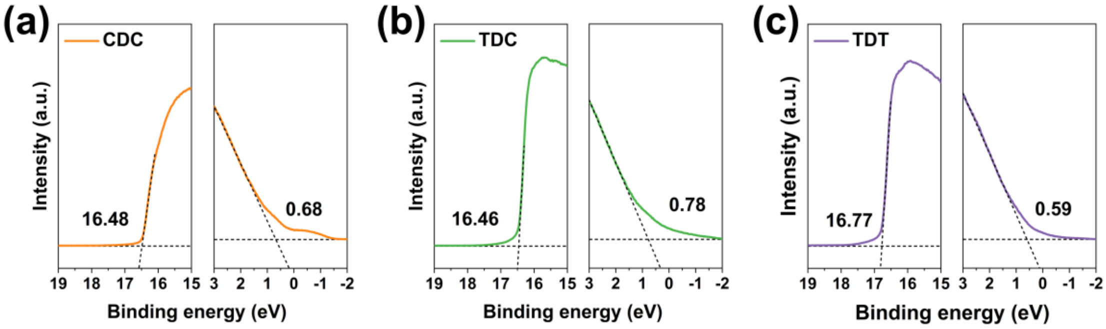

Figure S31. UPS spectra (using the He I lamp with a photon energy of 21.2 eV) of ITO/CDC, ITO/TDC and ITO/TDT substrates.

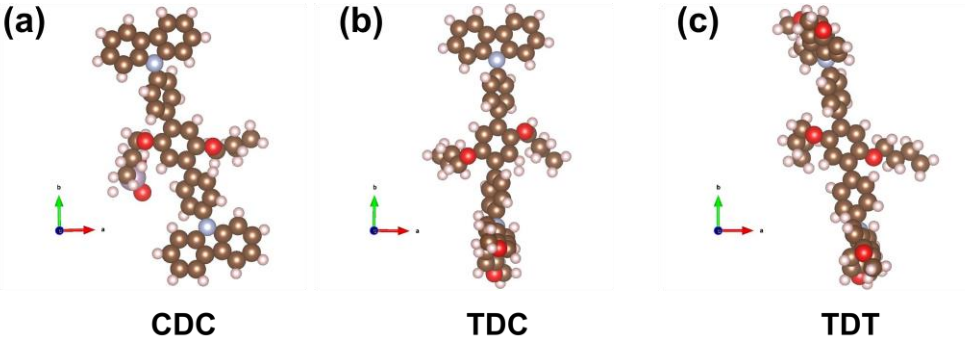

Figure S32. Top view and in-plane projection of D-SAMs adsorbed on ITO.

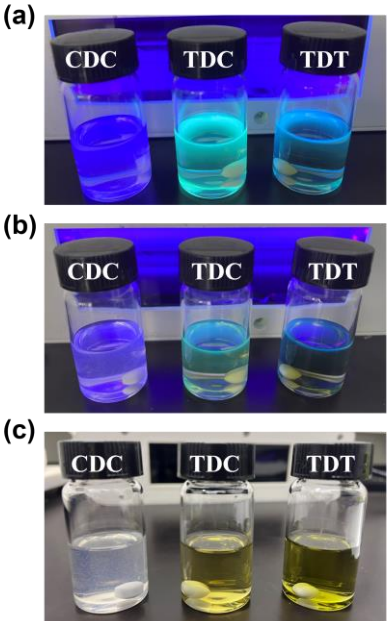

Figure S33. The D-SAM solution images of illuminate under (a) an ultraviolet lamp at 365nm, (b) an ultraviolet lamp at 254nm and (c) daily lighting.

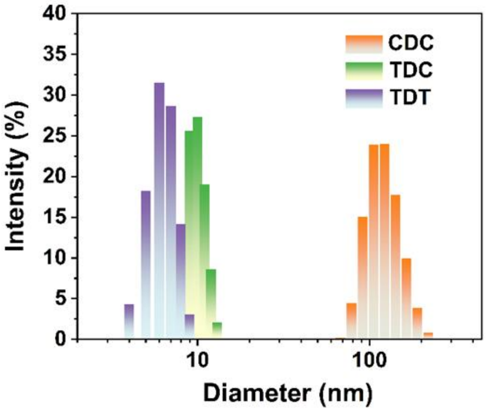

Figure S34. DLS patterns of CDC, TDC and TDT solutions.

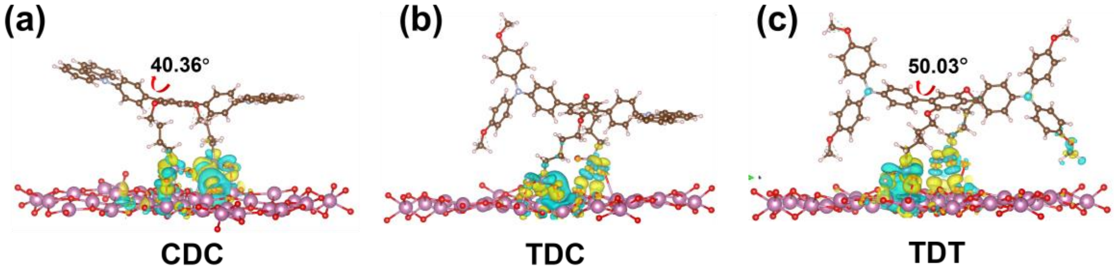

Figure S35. The bisphosphonate-anchored adsorption configurations of (a) CDC, (b) TDC and (c) TDT on the ITO surface.

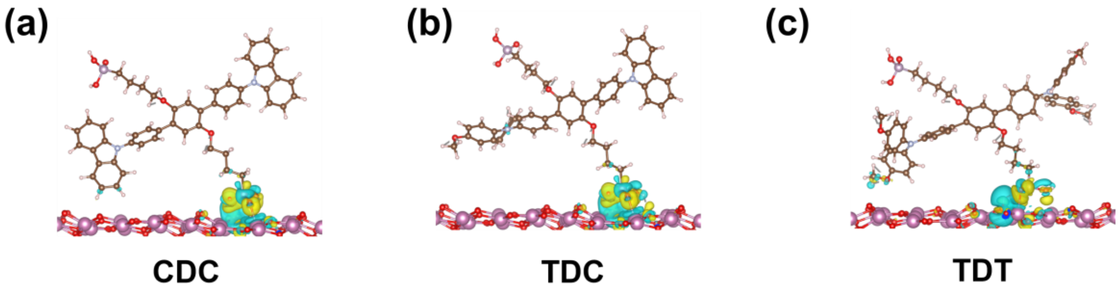

Figure S36. The monophosphate-anchored adsorption configurations of (a) CDC, (b) TDC and (c) TDT on the ITO surface.

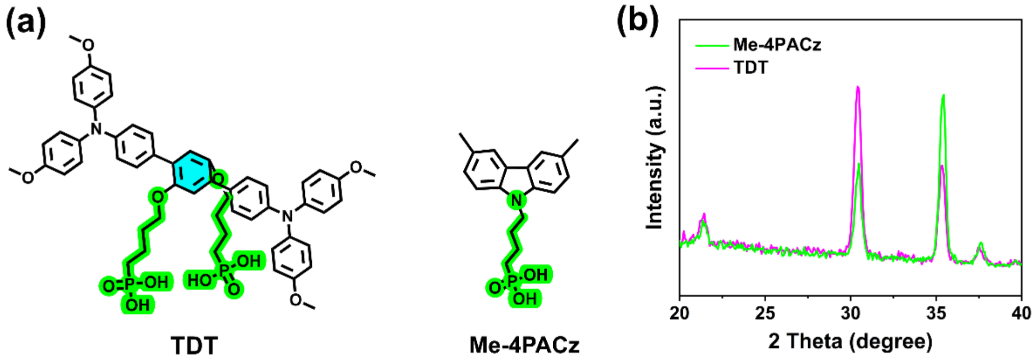

Figure S37. (a) The molecular structure of TDT and Me-4PACz. (b) Thin film GIXRD patterns of TDT and Me-4PACz deposited on ITO substrates.

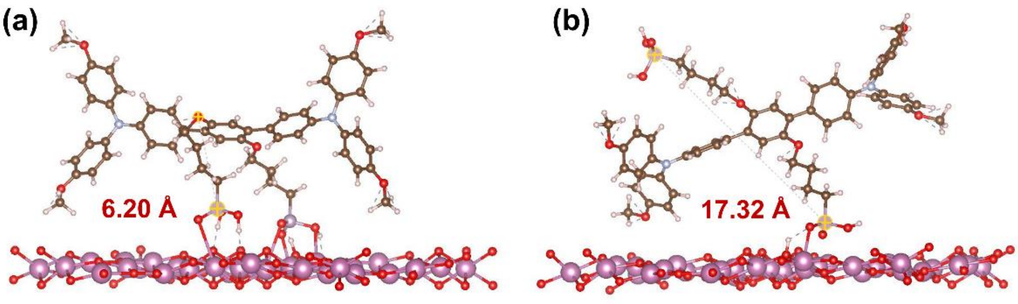

Figure S38. (a) The measured atomic distances in the face-on oriented and edge-on oriented configurations of TDT.

Figure S39. The PH digital images of (a) CDC, (b) TDC and (c) TDT in chloroform and methanol mixed solution (0.3 mmol L^{-1}).

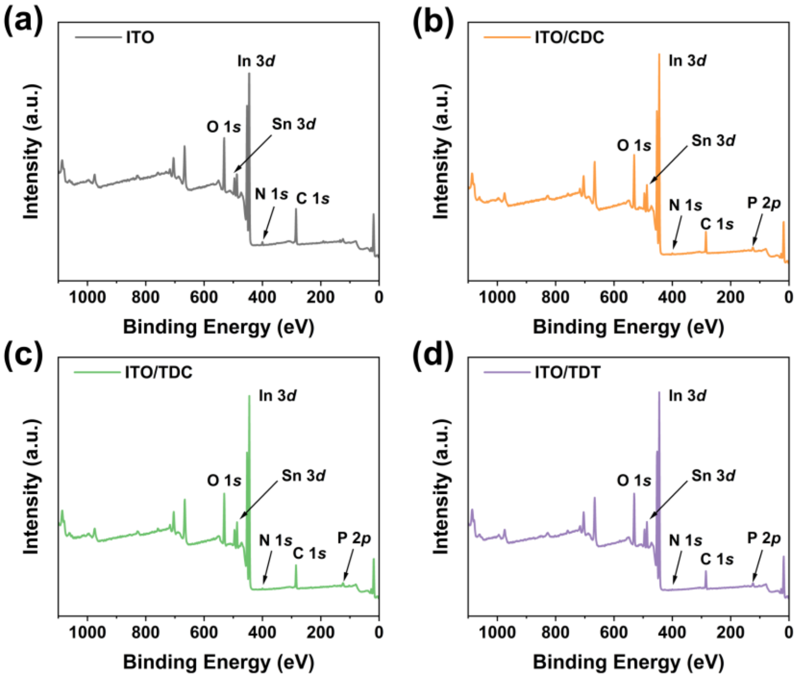

Figure S40. HR-XPS for ITO, ITO/CDC, ITO/TDC and ITO/TDT substrates.

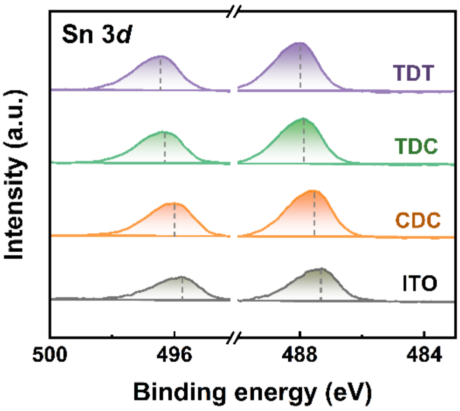

Figure S41. Sn 3*d* XPS spectra of bare ITO, ITO/CDC, ITO/TDC and ITO/TDT substrates.

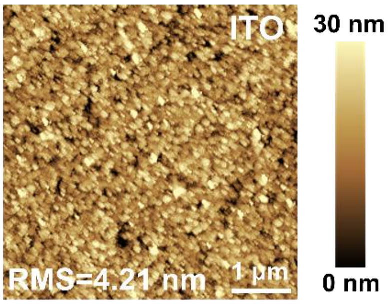

Figure S42. AFM measurement of the bare ITO.

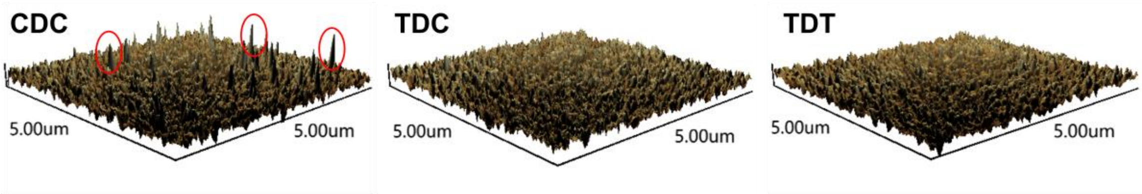

Figure S43. AFM 3D images of ITO/CDC, ITO/TDC and ITO/TDT films.

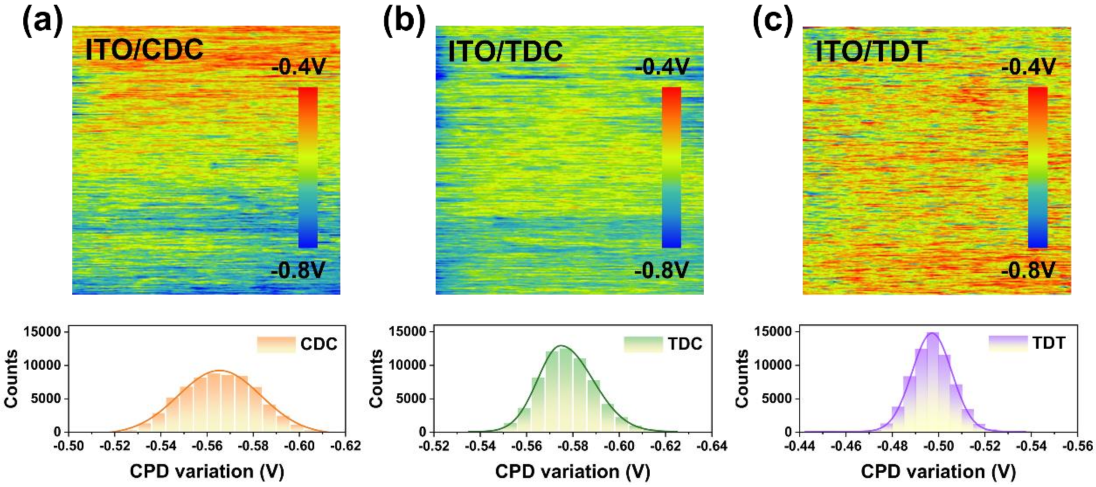

Figure S44. KPFM images and surface contact potential distributions of ITO/CDC, ITO/TDC and ITO/TDT films.

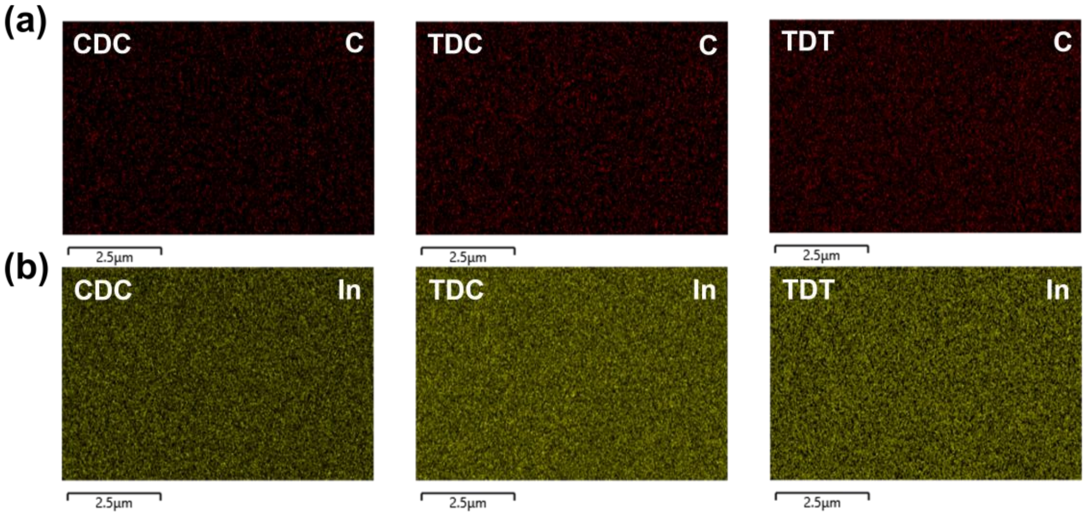

Figure S45. Elemental mapping of (a) C element and (b) In element for CDC, TDC, and TDT-modified ITO.

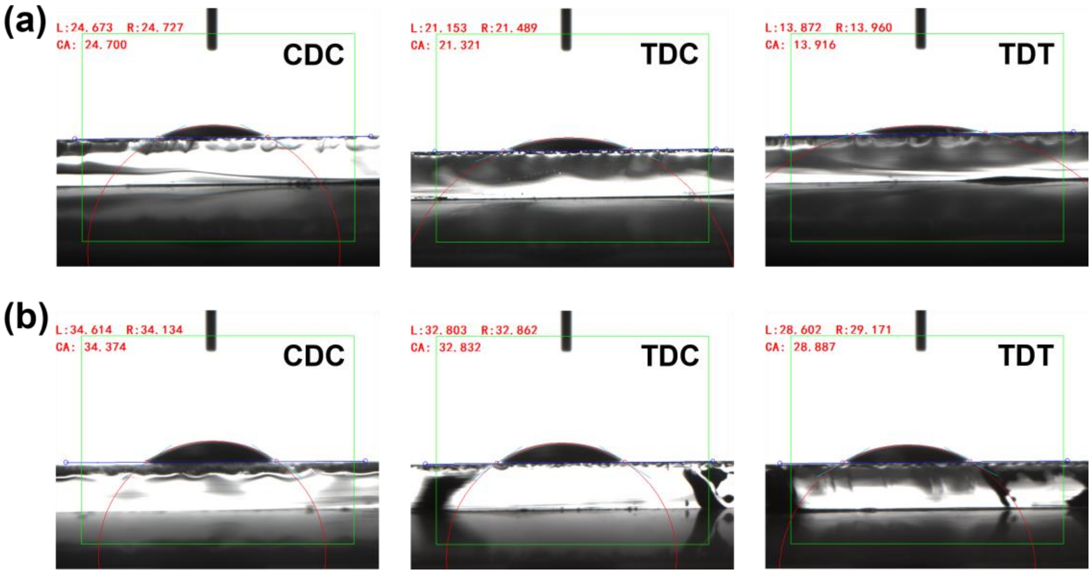

Figure S46. (a) Perovskite precursor solution and (b) water contact angles of CDC, TDC and TDT-treated ITO.

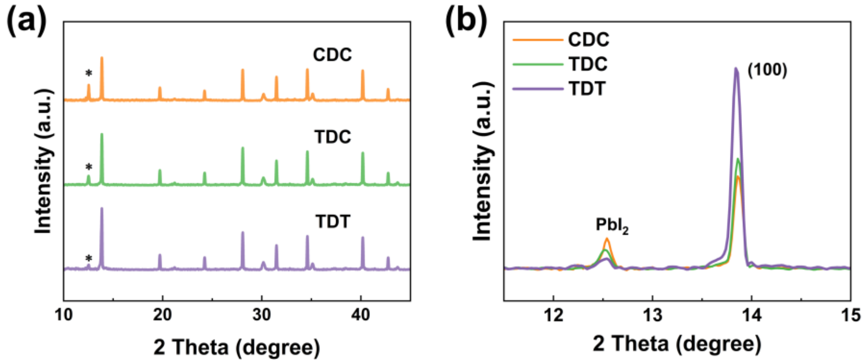

Figure S47. (a) XRD characteristic peaks of perovskite films and (b) magnified image (11.5°-15.0°) of perovskite films deposited on CDC, TDC and TDT substrates.

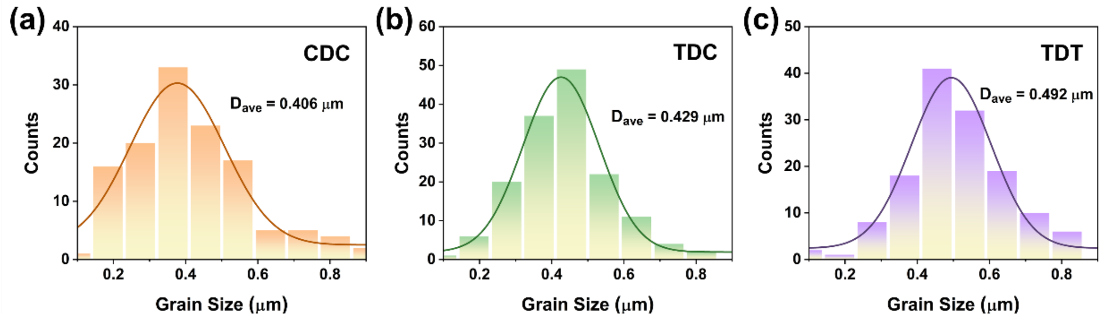

Figure S48. (a) CDC, (b) TDC and (c) TDT histograms of the corresponding particle size distributions of perovskite films.

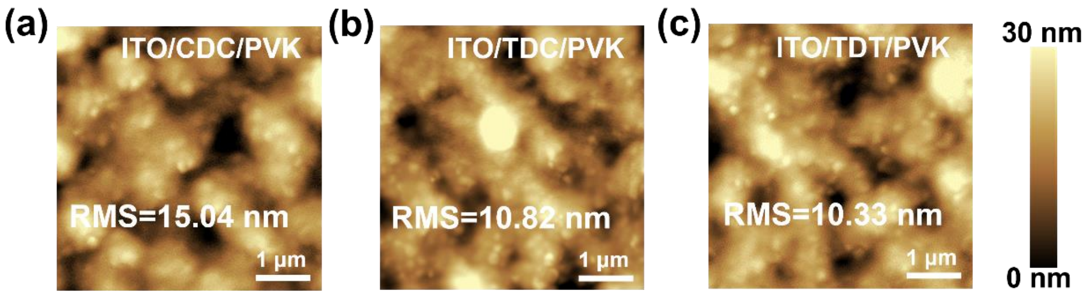

Figure S49. AFM morphology images of perovskite films deposited on (a) CDC, (b) TDC and (c) TDT show the root-mean-square roughness (RMS).

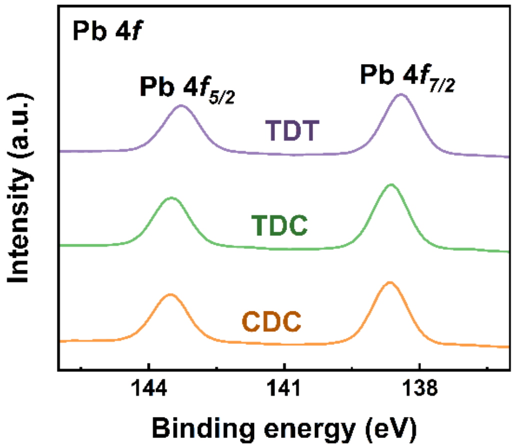

Figure S50. XPS of Pb 4*f* for perovskite films coated on different D-SAM-based substrates.

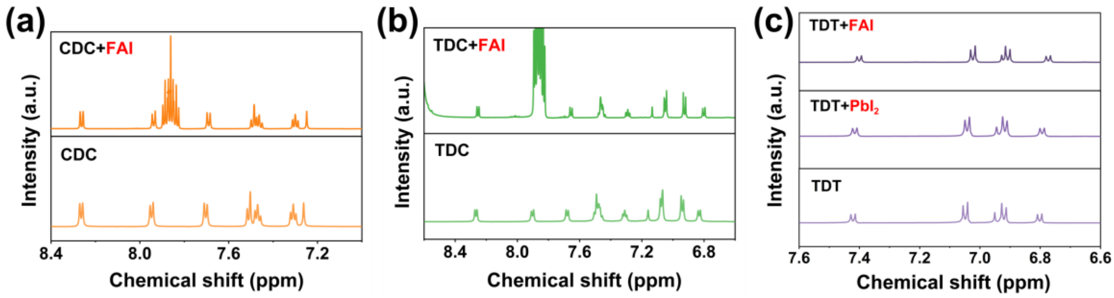

Figure S51. The ^{1}H NMR spectra of (a) pure CDC and CDC-FAI mixtures, (b) pure TDC and TDC-FAI mixtures and (c) pure TDT, TDT-PbI$_2$ and TDT-FAI mixtures dissolved in deuterated DMSO.

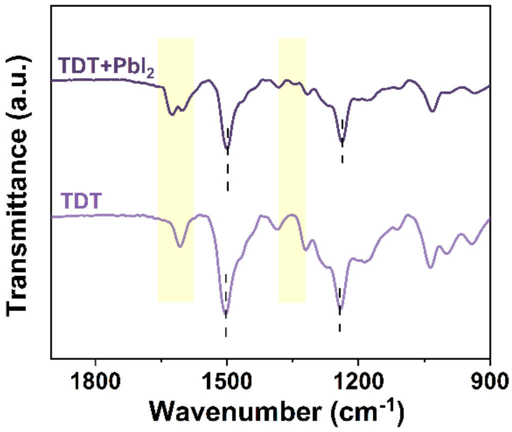

Figure S52. FTIR transmittance spectra of TDT and TDT-PbI$_2$ mixtures powder samples.

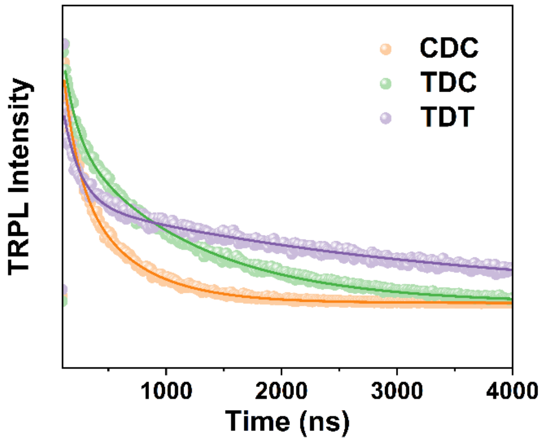

Figure S53. Time-resolved PL (TRPL) spectra of perovskite films deposited on ITO/D-SAM.

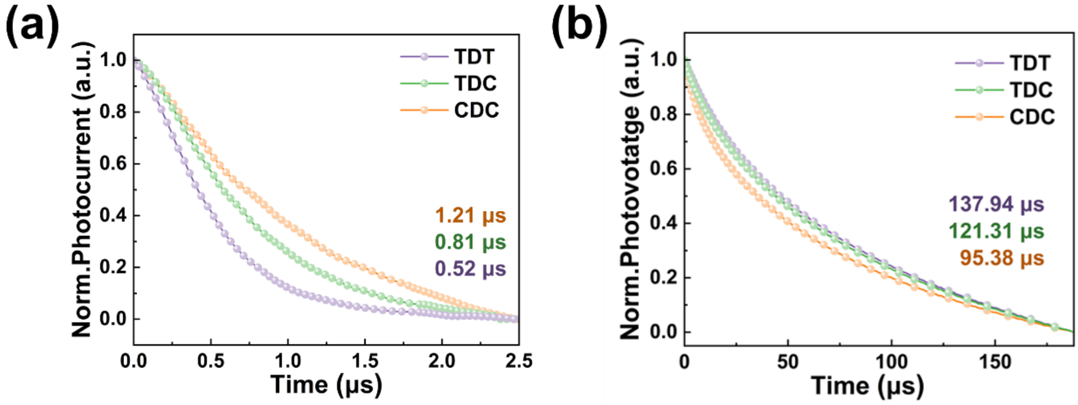

Figure S54. (a) TPC and (b) TPV decay curves of PSCs based on CDC, TDC and TDT films.

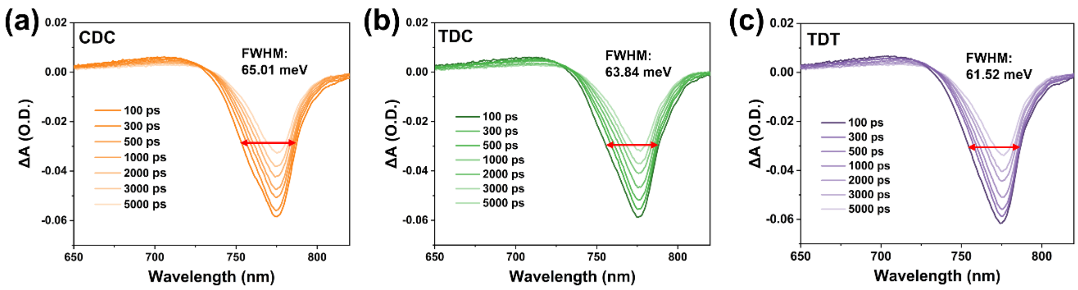

Figure S55. TA spectra at different delay times of the perovskite films coated on (a) CDC, (b) TDC and (c) TDT-based substrates.

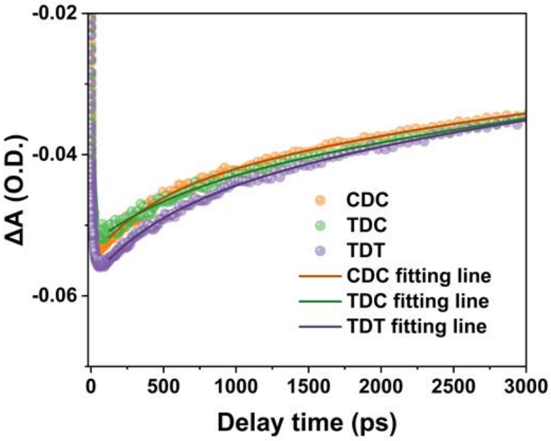

Figure S56. Corresponding fs-transient kinetics traces at the respective GSB maxima of the perovskite films.

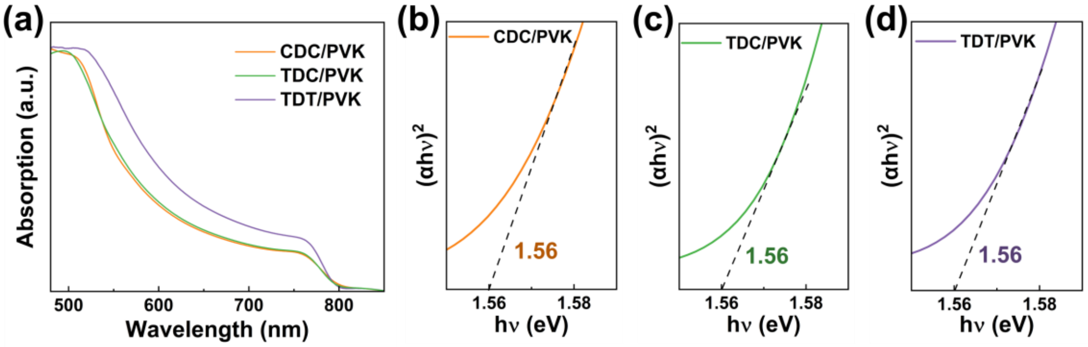

Figure S57. (a) UV-vis absorption spectra of the perovskite films. Tauc-plot curves of the perovskite films coated on (b) CDC, (c) TDC and (d) TDT-based substrates.

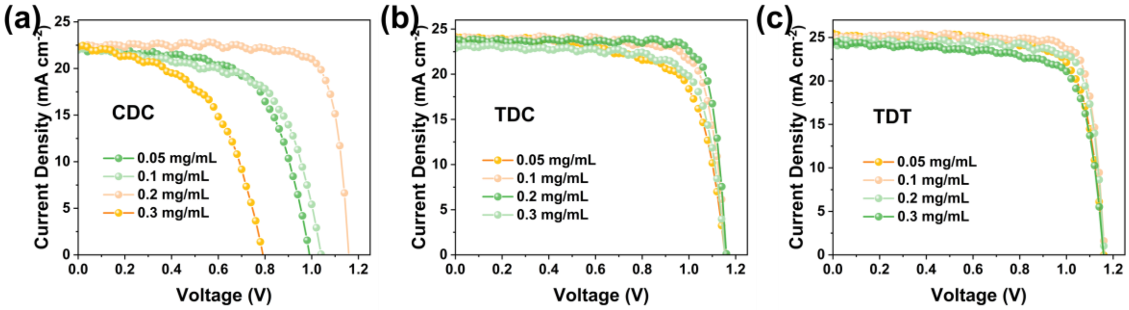

Figure S58. *J-V* curves of PSCs based on (a) CDC, (b)TDC and (c) TDT with varying concentrations.

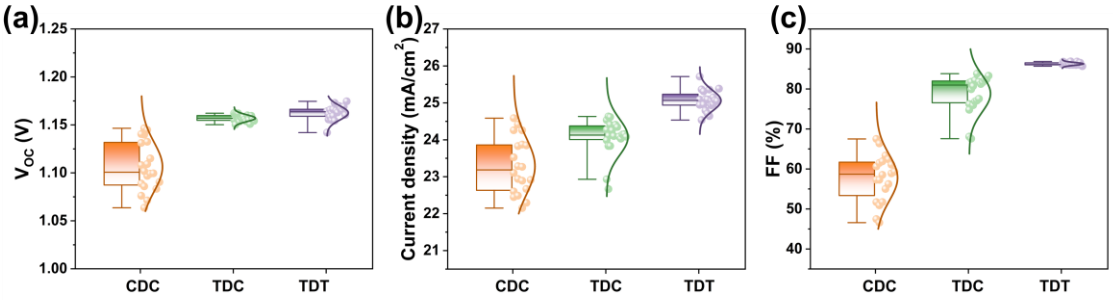

Figure S59. Statistical (a) V_{OC}, (b) J_{SC} and (c) *FF* of the PSCs of CDC, TDC and TDT.

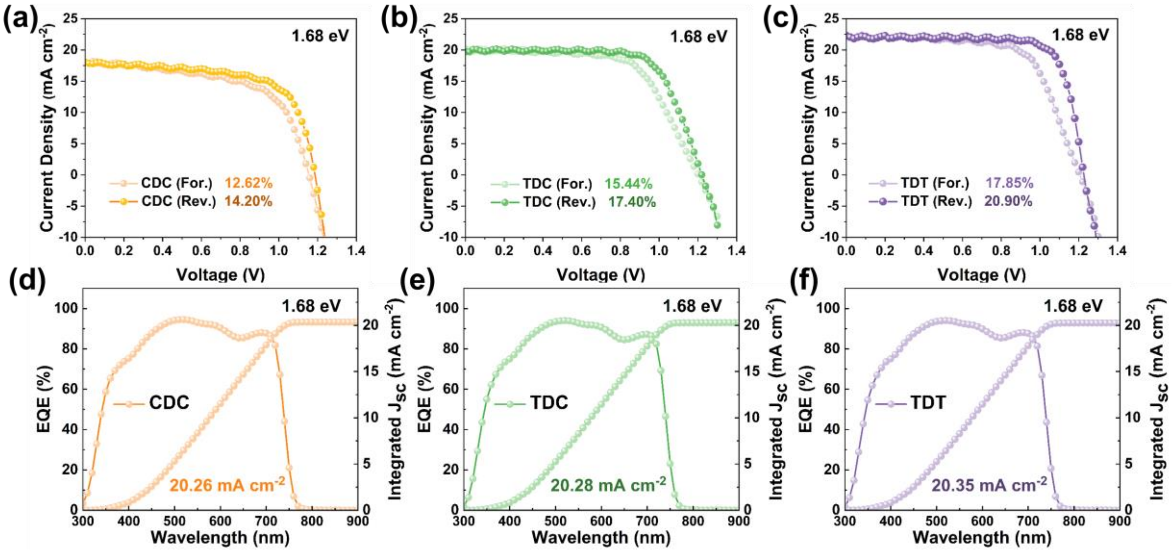

Figure S60. (a-c) The *J-V* and (d-f) EQE curves for Wide-Bandgap PSCs based on D-SAMs.

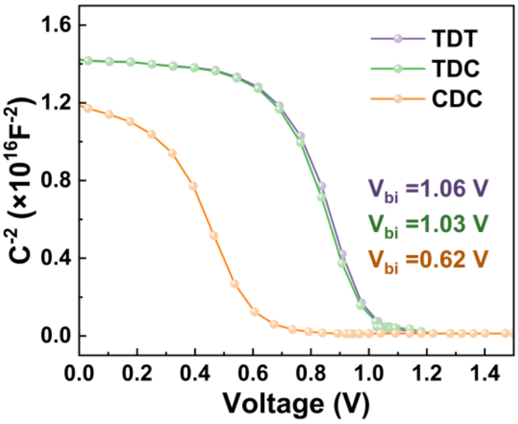

Figure S61. Mott–Schottky plots of CDC, TDC and TDT based PSCs. The curves on top of the data were extracted by linear fitting the drop region of Mott-Schottky plots, and V_{bi} was obtained via the intercept of the straight line with the x axis.

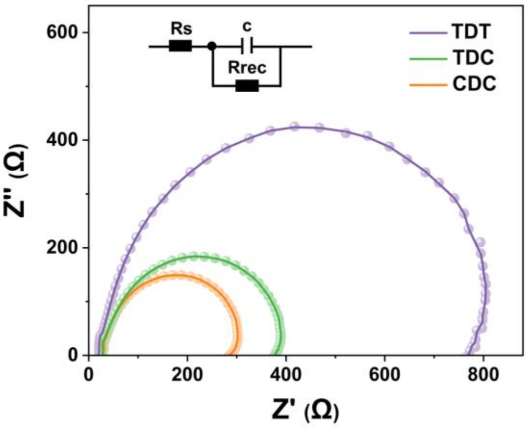

Figure S62. Electrochemical impedance spectra for CDC, TDC, TDT. The inset is the equivalent circuit, where R_s is the series resistance and R_{rec} is the charge recombination resistance, and the fitting results are expressed with solid lines in the Nyquist plots.

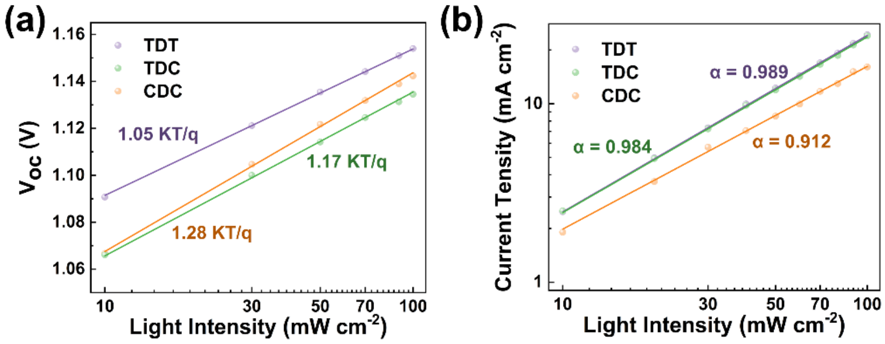

Figure S63. (a) V_{OC} and (b) J_{SC} versus light intensity for PSCs with CDC, TDC, and TDT.

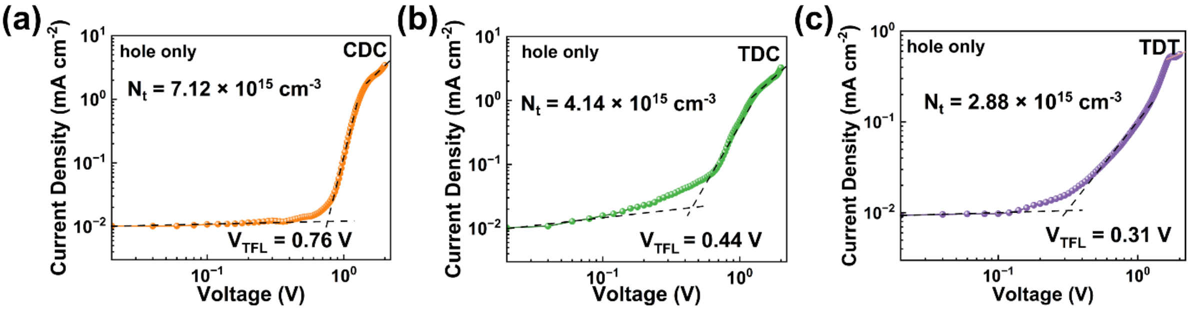

Figure S64. The space-charge-limited current (SCLC) versus voltage curves for the hole-only devices with configurations of ITO/D-SAM/perovskite/spiro-OMeTAD/Ag.

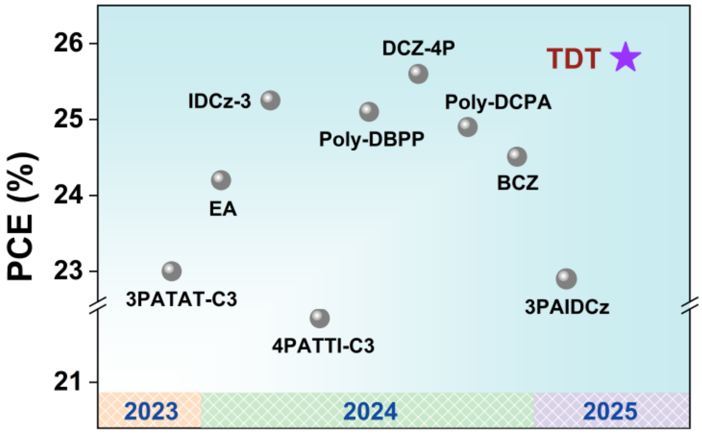

Figure S65. Efficiency of recently reported PSCs based on bisphosphonate-anchored, multi-phosphonate-anchored and polyphosphate-anchored SAMs.

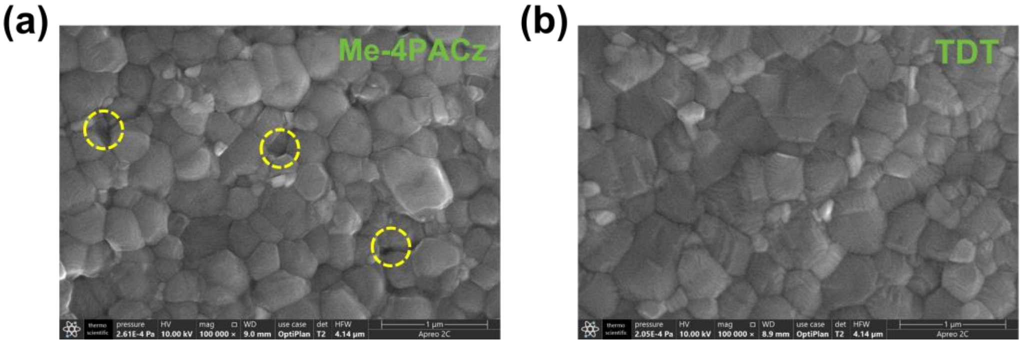

Figure S66. Top view SEM images of fresh (a) Me-4PACz and (b) TDT-treated perovskite films.

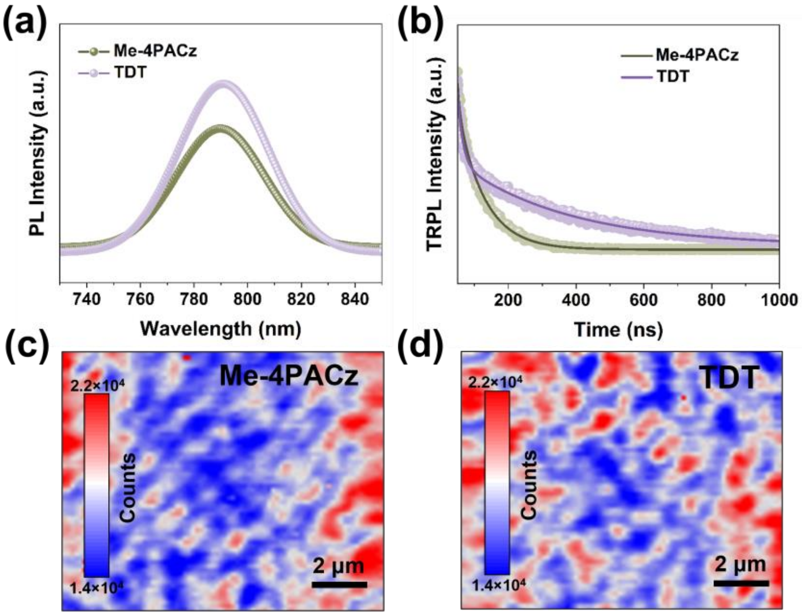

Figure S67. (a) Steady-state PL spectra, (b) Time-resolved PL (TRPL) spectra and (c) PL mapping of perovskite films deposited on Me-4PACz and TDT.

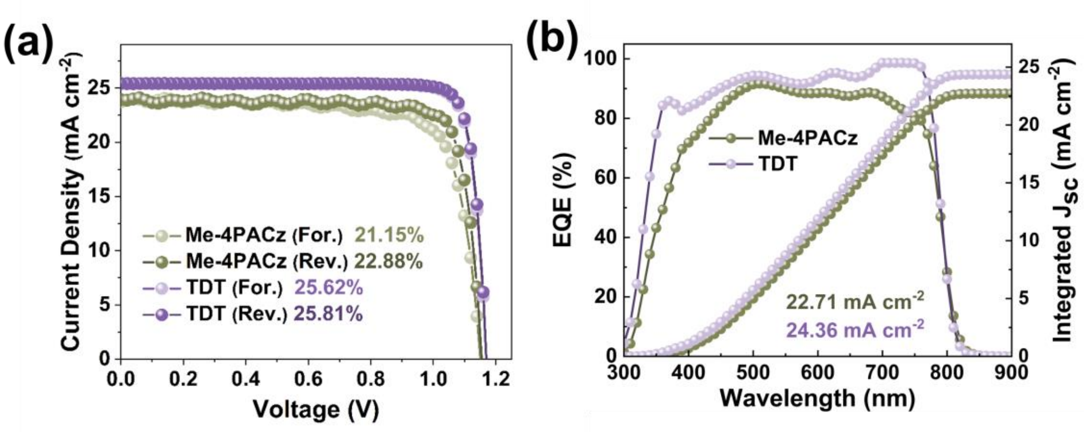

Figure S68. (a) The J-V and (b) EQE curves for Me-4PACz and TDT-based devices.

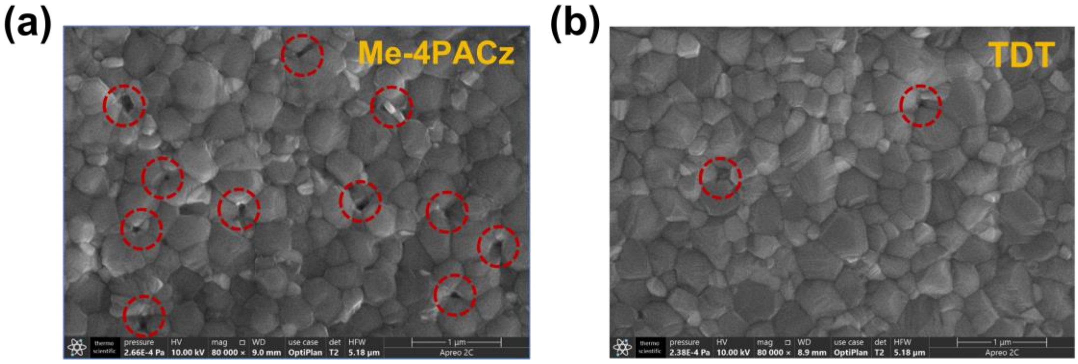

Figure S69. Top view SEM images of aged (a) Me-4PACz and (b) TDT-treated perovskite films.

Table S1. Efficiency of recently reported PSCs based on SAMs with multiple anchors.

Year	Type	SAM	Molecular Structure	PCE	Ref.
2023	p-i-n	3PATAT-C3	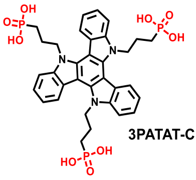 3PATAT-C3	23.00%	*J. Am. Chem. Soc.* **2023**, *145*, 7528–7539[15]
2024	p-i-n	IDCz-3	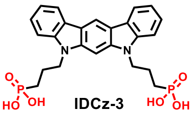 IDCz-3	25.15%	*Adv. Mater.* **2024**, *36*, 2401537[16]
2024	n–i–p	EA	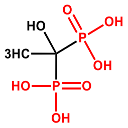 Etidronic acid	24.20%	*Adv. Funct. Mater.* **2024**, 2401391[17]
2024	p-i-n	4PATTI-C3	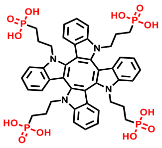 4PATTI-C3	21.70%	*Angew. Chem. Int. Ed.* **2024**, *63*, e202412939[18]
2024	n-i-p	BCZ	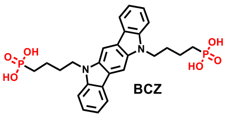 BCZ	24.51%	*Adv. Mater.* **2024**, *36*, 2308969[19]
2024	p-i-n	Poly-DBPP	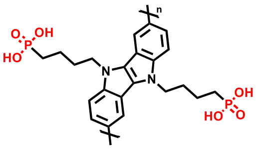 Poly-DBPP	25.1%	*Adv. Mater.* **2024**, *36*, 2412059[20]
2024	p-i-n	Poly-DCPA	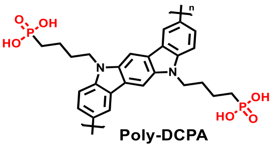 Poly-DCPA	24.9%	*Energy Environ. Sci.*, **2025**,*18*, 1366-1374[21]
2024	p-i-n	DCZ-4P	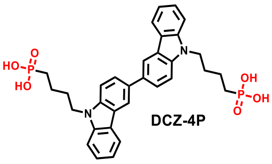 DCZ-4P	25.6%	*Nat Energy* 10, 181–190 (2025)[22]
2025	p-i-n	3PAIDCz	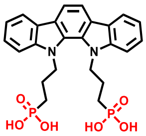 3PAIDCz	22.9% (flexible)	*Chemical Engineering Journal* 503 (2025) 158389[23]
2025	p-i-n	TDT	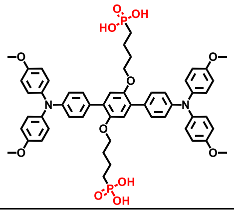	25.81%	This work

Table S2. Adsorption energy (E_{ads}) of ITO/CDC, ITO/TDC and ITO/TDT.

E_{ads}	CDC	TDC	TDT
Monophosphate-anchored	-1.164eV	-1.478eV	-1.633eV
Bisphosphate-anchored	-2.033eV	-2.432eV	-2.503eV

Table S3. The 2θ values obtained by GIXRD and the calculated d-space values.

2θ (°)	d-spacing (Å)
21.44	4.14
30.40	2.94
35.36	2.54
41.76	2.16

Table S4. C l*s* and In 3$d_{3/2}$ core-level peak area as measured by XPS for different D-SAM on ITO substrates. The C l*s* peak area is divided by the number of carbon atoms and a relative coverage factor is calculated by normalizing to the In 3$d_{3/2}$ core level area.

D-SAM	C 1*s* area	In 3$d_{3/2}$ area	Carbon atoms	Coverage factor
ITO/CDC	57075.25	1062270.55	50	1.08×10^{-3}
ITO/TDC	68406.73	1050452.3	52	1.25×10^{-3}
ITO/TDT	70092.85	997262.62	54	1.30×10^{-3}

Table S5. Element content data of D-SAMs modified-ITO surface from EDS measurements.

D-SAM	Element wt (%)							wt_C/wt_{In}	wt_P/wt_{In}
	C	N	O	P	In	Sn	Total		
ITO/CDC	9.70	0.00	35.89	0.53	42.68	11.20	100.00	0.227	0.012
ITO/TDC	10.10	0.60	36.81	0.55	41.04	10.90	100.00	0.246	0.013
ITO/TDT	10.90	0.42	35.78	0.64	41.25	11.01	100.00	0.264	0.016

Table S6. The fitting results of TRPL curves of perovskite films deposited on different substrates.

D-SAM	A_1 (%)	τ_1 (ns)	A_2 (%)	τ_2 (ns)	τ_{avg} (ns)
CDC	16.01	128.68	83.99	519.67	457.06
CDT	4.61	116.98	95.39	1074.57	1030.47
TDT	4.22	148.32	95.78	3215.91	3086.46

Table S7. Fitting parameters for TA spectra.

D-SAM	A_1	τ_1 (ps)	A_2	τ_2 (ps)	A_3	τ_3 (ps)
CDC	-0.00364	515.61	-0.01477	1970.50	-0.03994	19474.01
TDC	-0.00507	457.73	-0.01578	2208.75	-0.23924	21683.86
TDT	-0.00546	228.53	-0.01497	4168.44	-0.46919	43387.20

Table S8. Measured PLQY values and calculated QFLS parameters.

D-SAM	PLQY (%)	QFLS (eV)
CDC	1.56	1.305
TDC	2.35	1.315
TDT	2.47	1.317

Table S9. Photovoltaic performances of PSCs based on CDC with varying concentration.

Concentration (mg/ml)	V_{OC} (V)	J_{SC} (mA/cm^2)	*FF* (%)	PCE (%)
0.05	0.85	26.20	49.82	11.13
0.1	0.94	25.72	58.12	14.07
0.2	1.14	23.63	57.45	15.43
0.3	0.71	21.44	51.91	7.92
0.4	0.66	21.40	45.87	6.43
0.5	0.85	23.63	43.47	8.74
0.6	0.78	23.54	43.66	8.06

Table S10. Photovoltaic performances of PSCs based on TDC with varying concentration.

Concentration (mg/ml)	V_{OC} (V)	J_{SC} (mA/cm^2)	*FF* (%)	PCE (%)
0.03	1.14	23.79	76.03	20.66
0.05	1.16	23.96	82.05	22.81
0.1	1.16	23.49	81.63	22.17
0.2	1.16	23.89	84.26	23.33
0.3	1.16	23.52	81.53	22.15
0.4	1.15	22.67	81.66	21.53
0.5	1.15	23.69	77.38	21.02
0.6	1.15	23.07	82.99	22.02
0.8	1.01	25.41	64.60	16.53
1	1.15	22.54	75.61	19.67

Table S11. Photovoltaic performances of PSCs based on TDT with varying concentration.

Concentration (mg/ml)	V_{OC} (V)	J_{SC} (mA/cm^2)	*FF* (%)	PCE (%)
0.02	1.16	23.89	84.256	23.33
0.04	1.16	23.52	81.53	22.15
0.06	1.17	25.42	84.29	25.12
0.08	1.17	24.63	85.93	24.69
0.1	1.17	25.37	86.44	25.65
0.2	1.17	25.47	86.21	25.37
0.3	1.17	24.63	85.93	24.69
0.4	1.16	23.83	82.14	22.71
0.5	1.15	25.49	81.51	23.94
0.6	1.16	24.71	81.87	23.47
0.8	1.16	23.27	81.78	22.04
1	1.15	22.67	81.66	21.36

Table S12. Photovoltaic performances of the TDT-based PSCs with varying thermal annealing time.

Annealing time (min)	V_{OC} (V)	J_{SC} (mA/cm^2)	*FF* (%)	PCE (%)
5	1.15	24.22	85.47	23.92
10	1.17	25.60	85.64	25.68
15	1.16	24.75	83.11	23.89
20	1.15	24.03	82.43	22.88
25	1.16	24.46	83.84	23.49

Table S13. Photovoltaic performances of the TDT-based PSCs with varying thermal annealing temperature.

Annealing temperature (°C)	V_{OC} (V)	J_{SC} (mA/cm^2)	*FF* (%)	PCE (%)
80	1.16	24.41	82.49	23.30
90	1.15	24.82	80.71	23.15
100	1.17	25.62	85.11	25.46
110	1.16	24.76	83.54	24.07
120	1.16	24.46	83.84	23.79

Table S14. Photovoltaic parameters of best-performing Wide-Bandgap PSCs based on CDC, TDC, and TDT as the HTLs.

D-SAM	Scanning direction	V_{OC} [V]	J_{SC} [mA/cm^2]	*FF* (%)	PCE$_{max}$ (%)	$J_{SC}{}^a$ [mA/cm^2] [a]
CDC	Reverse	1.187	17.99	66.53	14.20	20.26
	Forward	1.156	18.04	60.53	12.62	
TDC	Reverse	1.220	19.90	71.65	17.40	20.28
	Forward	1.202	20.05	64.05	15.44	
TDT	Reverse	1.226	22.09	77.15	20.90	20.35
	Forward	1.206	22.28	66.44	17.85	

[a] The J_{SC} values calculated from the EQE spectra.

Table S15. Specific fitting results of Nyquist plots using the Z-view software.

D-SAM	R_s (Ω)	R_{rec} (Ω)
CDC	28.81	288.26
TDC	28.15	378.69
TDT	20.34	772.42

Table S16. The fitting results of TRPL curves of perovskite films deposited on Me-4PACz and TDT modified substrates.

D-SAM	A_1 (%)	τ_1 (ns)	A_2 (%)	τ_2 (ns)	τ_{avg} (ns)
Me-4PACz	1.99	71.56	98.01	770.13	756.23
TDT	4.22	148.32	95.78	3215.91	3086.46

Reference

1 G. Kresse, J. Furthmüller, *Comput. Mater. Sci.* 1996, **6**, 15-50.

2 G. Kresse, D. Joubert, *Phys. Rev. B* 1999, **59**, 1758-1775.

3 J. P. Perdew, K. Burke, M. Ernzerhof, *Phys. Rev. Lett.* 1996, **77**, 3865-3868.

4 W. He, Z. Lin, K. Zhao, Y. Li, C. Meng, J. Li, S. Lee, Y. Wu, X. Hao, *Adv. Mater.* 2022, **34**, 2203920.

5 H. Wang, Q. Zhang, Z. Lin, H. Liu, X. Wei, Y. Song, C. Lv, W. Li, L. Zhu, K. Wang, Z. Cui, L. Wang, C. Lin, P. Yin, T. Song, Y. Bai, Q. Chen, S. Yang, H. Chen, *Sci. Bull.* 2024, **69**, 1050-1060.

6 J. Zheng, Z. Ying, Z. Yang, Z. Lin, H. Wei, L. Chen, X. Yang, Y. Zeng, X. Li, J. Ye, *Nat. Energy* 2023, **8**, 1250-1261.

7 Q. Zhang, H. Liu, X. Wei, Y. Song, C. Lv, W. Li, L. Zhu, Y. Lan, Y. Du, K. Wang, P. Yin, C. Lin, Z. Lin, Y. Bai, Q. Chen, S. Yang, H. Chen, *Small* 2024, **20**, 2402061.

8 Z. Li, C. Wang, P.-P. Sun, Z. Zhang, Q. Zhou, Y. Du, J. Xu, Y. Chen, Q. Xiong, L. Ding, M. K. Nazeeruddin, P. Gao, *Nano Energy* 2022, **100**, 107468.

9 Y. Luo, J. Zhu, X. Yin, W. Jiao, Z. Gao, Y. Xu, C. Wang, Y. Wang, H. Lai, H. Huang, J. Luo, J. Wang, J. You, Z. Zhang, X. Hao, G. Zeng, S. Ren, Z. Li, F. Fu, M. Li, C. Xiao, C. Chen, D. Zhao, *Adv. Energy Mater.* 2024, **14**, 2304429.

10 C. Zhang, Y. Son, H. Kim, S.-H. Lee, X. Liang, G. Fu, S.-U. Lee, D.-A. Park, Q. Jiang, K. Zhu, N.-G. Park, *Joule* 2024, **8**, 1394-1411.

11 O. Almora, C. Aranda, E. Mas-Marzá, G. Garcia-Belmonte, *Appl. Phys. Lett.* 2016, **109**, 173903.

12 M. Stolterfoht, P. Caprioglio, C. M. Wolff, J. A. Márquez, J. Nordmann, S. Zhang, D. Rothhardt, U. Hörmann, Y. Amir, A. Redinger, L. Kegelmann, F. Zu, S. Albrecht, N. Koch, T. Kirchartz, M. Saliba, T. Unold, D. Neher, *Energy Environ. Sci.* 2019, **12**, 2778-2788.

13 S. Liu, J. Li, W. Xiao, R. Chen, Z. Sun, Y. Zhang, X. Lei, S. Hu, M. Kober-Czerny, J. Wang, F. Ren, Q. Zhou, H. Raza, Y. Gao, Y. Ji, S. Li, H. Li, L. Qiu, W. Huang, Y. Zhao, B. Xu, Z. Liu, H. J. Snaith, N.-G. Park, W. Chen, *Nature* 2024, **632**, 536-542.

14 Q. Dong, Y. Fang, Y. Shao, P. Mulligan, J. Qiu, L. Cao, J. Huang, *Science* 2015, **347**, 967-970.

15 M. A. Truong, T. Funasaki, L. Ueberricke, W. Nojo, R. Murdey, T. Yamada, S. Hu, A. Akatsuka, N. Sekiguchi, S. Hira, L. Xie, T. Nakamura, N. Shioya, D. Kan, Y. Tsuji, S. Iikubo, H. Yoshida, Y. Shimakawa, T. Hasegawa, Y. Kanemitsu, T. Suzuki, A. Wakamiya, *J. Am. Chem. Soc.* 2023, **145**, 7528-7539.

16 J. Wu, P. Yan, D. Yang, H. Guan, S. Yang, X. Cao, X. Liao, P. Ding, H. Sun, Z. Ge, *Adv. Mater.* 2024, **36**, 2401537.

17 Y. Zhang, T. Kong, Y. Liu, X. Liu, W. Liu, M. Saliba, D. Bi, *Adv. Funct. Mater.* 2024, **34**, 2401391.

18 M. A. Truong, L. Ueberricke, T. Funasaki, Y. Adachi, S. Hira, S. Hu, T. Yamada, N. Sekiguchi, T. Nakamura, R. Murdey, S. Iikubo, Y. Kanemitsu, A. Wakamiya, *Angew. Chem. Int. Ed.* 2024, **63**, e202412939.

19 X. Li, W. Wang, K. Wei, J. Deng, P. Huang, P. Dong, X. Cai, L. Yang, W. Tang, J. Zhang, *Adv. Mater.* 2024, **36**, 2308969.

20 F. Wang, T. Liu, Y. Liu, Y. Zhou, X. Dong, Y. Zhang, X. Shi, Y. Dou, Z. Ren, L. Wang, Y. Zhao, S. Luo, X. Hu, X. Peng, C. Bao, W. Wang, J. Wang, W. Hu, S. Chen, *Adv. Mater.* 2024, **36**, 2412059.

21 Y. Zhao, Y. Liu, Z. Ren, Y. Li, Y. Zhang, F.-C. Kong, T. Liu, X. Shi, Y. Dou, L. Wang, F. Wang, X. Guo, Y. Cao, W. Wang, P. C. Y. Chow, S. Chen, *Energy Environ. Sci.* 2025, **18**, 1366-1374.

22 J. Chen, X. Wang, T. Wang, J. Li, H. Y. Chia, H. Liang, S. Xi, S. Liu, X. Guo, R. Guo, Z. Jia, X. Yin, Q. Zhou, Y. Wang, Z. Shi, H. Zhou, D. Lai, M. Zhang, Z. Xing, W. R. Leow, W. Yan, Y. Hou, *Nat. Energy* 2025, **10**, 181-190.

23 S. Tu, W. Chen, Y. Gang, Q. Xiong, X. Li, *Chem. Eng. J.* 2025, **503**, 158389.